PERGAMON

International Journal of Multiphase Flow 26 (2000) 663–715

International Journal of Multiphase Flow

www.elsevier.com/locate/ijmulflow

Characterization of fluidization regimes by time-series analysis of pressure fluctuations

F. Johnsson [a,*], R.C. Zijerveld [b], J.C. Schouten [b], C.M. van den Bleek [b], B. Leckner [a]

[a] *Department of Energy Conversion, School of Mechanical Engineering, Chalmers University of Technology, S-412 96, Göteborg, Sweden*

[b] *Department of Chemical Process Technology, Faculty of Chemical Technology and Materials Science, Delft University of Technology, Julianalaan 136, 2628 BL, Delft, The Netherlands*

Received 4 August 1997; received in revised form 17 April 1999

Abstract

This work compares time, frequency and state-space analyses of pressure measurements from fluidized beds. The experiments were carried out in a circulating fluidized bed, operated under ambient conditions and under different fluidization regimes. Interpretation of results in time domain, such as standard deviation of the pressure fluctuations, may lead to erroneous conclusions about the flow regime. The results from the frequency domain (power spectra) and state-space analyses (correlation dimension, D_{ML}, and Kolmogorov entropy, K_{ML}, together with a non-linearity test) of the pressure fluctuations are generally in agreement and can be used complementary to each other. The power spectra can be divided into three regions, a region corresponding to the macro-structure (due to the bubble flow) and, at higher frequencies, two regions representing finer structures that are not predominantly governed by the macro structure of the flow. In all fluidization regimes, the measured pressure fluctuations exhibited an intermittent structure, which is not revealed by power spectral analysis of the original signals. Fluctuations with pronounced peaks in the power spectrum and in the auto-correlation function, corresponding to passage of single bubbles through the bed, are non-linear with a low dimension ($D_{ML} < 5.5$). For $D_{ML} < 5.5$, the Kolmogorov entropy is proportional to the amount of energy in the spectral range of the intermittent structures observed, whereas for $D_{ML} > 5.5$ both K_{ML} (bits/cycle) and D_{ML} are insensitive to changes in the distribution of energy in power spectra. Thus, the state-space analysis reflects that non-linearity is mostly found in the macro-structure of the flow. Fluidized bed time series treated in this work are available at http://www.entek.chalmers.se/~fijo

Keywords: Fluidized bed; Fluidization; Regimes; Pressure; Fluctuation; Time-series analysis; Non-linear; Chaos

* Corresponding author.

0301-9322/00/$ - see front matter
PII: S0301-9322(99)00028-2

1. Introduction

This work deals with analysis of time series of pressure signals measured in fluidized beds. The aim is to compare available methods of time-series analysis by applying these on pressure signals recorded at different fluidization regimes. The paper is directed to readers interested in hydrodynamics of two-phase flow, especially fluidization, and methods of time-series analysis are only briefly described. For details on these methods the references given should be consulted.

Such a comparison of the characterization of hydrodynamics of fluidized beds is necessary, since, in spite of numerous results available from investigations on the characterization of the hydrodynamics of fluidized beds (summarized in the reviews of, e.g., Yerushami and Avidan, 1985; Bi and Fan, 1992), these results were obtained under different conditions and are difficult to compare. One of the important reasons for the difficulty of interpretation of results lies in the data analysis and, therefore, this subject in particular should be further studied.

1.1. Experimental methods and data analysis

Several methods have been proposed for characterization of fluidization regimes: visual observations, study of time averaged entities such as the axial solids concentration profile and interpretation of fluctuating signals from in-bed measurements.

For a qualitative classification of regimes visual observation is important, but subjective in nature; what is regarded to be a turbulent regime by some observers may be described as bubbling by others. In quantitative measurements, frame by frame analysis of motion pictures has been used to determine bubble and cluster velocities and bubble frequency (e.g., Newby and Keairns, 1986; Yang et al., 1986). Although recent developments in video techniques make such an analysis easier, it is still a tedious method.

Changes in the vertical distribution of time-averaged solids concentration (from pressure drop measurements) have been used as an indirect measure of the bed dynamics. For example, an S-shaped profile was related to the fast fluidization regime by Li and Kwauk (1980). A change in conditions, which results in the disappearance of the S-shaped profile, is then interpreted as a transition either to pneumatic transport (increase in velocity and/or decrease in solids flux), or to the bubbling regime (decrease in velocity and/or increase in solids flux). A change in solids concentration or bubble volume fraction with a change in the operating condition has also been used to identify a regime transition (e.g., Canada et al., 1978; Avidan and Yerushalmi, 1982). The solids concentration is then recorded in a certain point or in a certain region of the bed. Methods based on the study of time averaged values of solids concentration do not directly quantify the flow dynamics and may lead to pitfalls.

A quantitative description of flow regimes can be obtained from time-series analysis of fluctuating signals of in-bed measurements of pressure (gauge or differential pressure) or of other signals, such as local solids concentration (from optical and capacitance probes). The key to such a quantification is an appropriate measurement method, as well as appropriate methods of time-series analysis of the measured fluctuating signals. Time-series analysis for this purpose operate in time domain, frequency domain or in state-space, the latter being used in non-linear time-series analysis.

1.1.1. Methods based on time domain analysis

The simplest analysis in time domain is to plot a sequence of data points of the measured signal. This gives a qualitative description of the time scale and of the complexity of the flow. In most fluidized bed systems, the main frequencies are of the order of 1–5 Hz, and a sequence of 10 s is suitable for this purpose.

The most common method in time domain is to study the amplitude of signals (usually pressure), expressed as standard deviation or variance (viz., second order statistical moment). The change in amplitude with operating conditions has been of interest for identification of transitions between regimes rather than quantifying the dynamics. This method has several drawbacks, which are mainly linked to the problem of defining the operating condition. A maximum in the standard deviation versus fluidization velocity is often employed as a criterion for transition to turbulent fluidization (velocities of onset of transition, u_c, and onset to turbulent fluidization, u_k) or for identification of the transport velocity, u_{tr} (the velocity at which all solids introduced into the riser are transported up through the riser in fully entrained flow). Bi and Fan (1992) have summarized investigations, which were mainly based on this method. Rhodes and Geldart (1986) questioned the above interpretation of the maximum in standard deviation, and claimed that u_k instead represents the velocity at which the bed height becomes zero when the velocity is increased. From the comparison of the reported observations Bi and Fan concluded that u_k represents a transition, but only for Group A particles ($Ar < 125$, ambient conditions, Ar is the Archimedes number), whereas for Group B particles ($Ar > 125$) u_k equals the transport velocity u_{tr}, i.e., in the latter case the conclusion is similar to that of Rhodes and Geldart (although exact comparisons are difficult to make since determination/definition of u_{tr} varies somewhat between investigations).

Johnsson et al. (1995) showed that caution has to be taken when using the amplitude as a method for detection of fluidization regimes. It was found, with Group B particles, that a maximum in the curve of amplitude vs. velocity may indeed be a result of a transition to a turbulent fluidization regime, but it could also be caused by a redistribution of bed material from the riser side to the cyclone side, while the fluidization regime remains the same. This was concluded from a comparison of power spectra of in-bed pressure signals at different fluidization velocities in units of different geometry; non-circulating as well as circulating beds. Hence, the amplitude alone is not sufficient to quantify the bed dynamics and in some cases can be misleading.

Another problem with defining u_c and u_k from the amplitude of bed-pressure fluctuations is the dependence on measurement method. Johnsson et al. (1992) showed that if the amplitude of measured differential in-bed pressure fluctuations was normalized with the bed pressure drop, it was not possible to define the transition velocities u_c and u_k under the conditions studied; no maximum was found in spite of the existence of a maximum of the standard deviation when plotted vs. velocity. A general discussion on the influence of measurement method was recently made by Bi and Grace (1995). They concluded that u_c is a strong function of measurement method (results obtained from absolute pressure fluctuations differ from those of differential pressure fluctuations), while u_k depends on the configuration of the solids recycle system.

In summary, characterization of the regime by amplitude is, apart from not giving information about the time scale, influenced by the dynamics of the flow, by the distribution of

bed material in the system, and by changes in the average suspension density. Since the link between these three effects is unknown, this measure of fluidized bed hydrodynamics should be applied with great care.

Higher order moments, i.e., skewness (normalized third-order statistical moment), S, and flatness (normalized fourth-order statistical moment, also called kurtosis), F, which express lack of symmetry ($S = 0$ for a Gaussian distribution) and sharpness in a probability distribution ($F = 3$ for a Gaussian distribution), have been applied by a few authors for determination of regime transitions, in particular, u_c and/or u_k. Lee and Kim (1988) calculated values of skewness from time series of absolute pressure fluctuations. They observed a shift from negative to positive skewness and a maximum in flatness with an increase in velocity, and considered the zero point in skewness and the flatness-maximum to correspond to the transition velocity u_c. However, Bi and Grace (1995) compared regime transitions based on skewness and amplitude from time series of absolute and differential pressure and optical probes. Their transition results differed depending on whether they used skewness or amplitude, and also depending on the type of measurement.

In intermittent time series, when the high-frequency activity comes in bursts separated by relatively long quiescent periods (low amplitude fluctuations), the flatness can also be seen as the ratio of the time spent under quiescent conditions to the time spent under active conditions. A typical example is a signal from a hot-wire anemometer in a turbulent gas-flow which, when high-pass filtered, is strongly intermittent (e.g., Frisch and Morf, 1981). Intermittent behavior can be a characteristic of non-linear systems (Frisch and Morf, 1981; Manneville, 1981; Greenside et al., 1982; Provenzale et al., 1993). It should, however, be noted that highly intermittent systems give time series which, when not high-pass filtered, may yield a flatness, F, which is close to that of a Gaussian distribution, $F \approx 3$ (e.g., Batchelor, 1959), and the intermittent structure is normally not revealed until high-pass filtering is performed.

1.1.2. Frequency domain analysis

Analysis of frequency distribution (e.g., by Fast Fourier Transform, FFT) has been applied on time series of pressure and solids concentration from fluidized beds. In bubbling and slugging beds, the dominant frequency in a power spectrum is that at which the bubbles/slugs pass through the bed (Verloop and Heertjes, 1974; Broadhurst and Becker, 1976; Fan et al., 1981; Satija and Fan, 1985; Sun et al., 1994). Regime transitions were identified by a change in frequency distribution in power spectra (Lirag and Littman, 1971; Canada et al., 1978; Satija and Fan, 1985; Satija et al., 1985; Johnsson et al., 1995; Svensson et al., 1996a). The interpretation of power spectra is subjective. What is regarded to be a peak for determination of a dominant frequency may differ between observers. The shape of a spectrum depends on the number of samples, the sampling frequency and the number of spectra averaged; given a certain number of samples, there is a trade-off between the statistical significance and the frequency resolution of the spectrum.

Frequency spectra may give a quite different picture from that of amplitude analysis. Johnsson et al. (1995) studied regimes in fluidized-bed units of different geometries. All units gave a maximum in the amplitude of the pressure fluctuations. In the units where a transition of regimes of fluidization actually took place, there was a pronounced change in the frequency distribution over the transition region from the bubbling bed regime to much wider spectra in

the turbulent regime. In the units which showed no transition, there was little change in the frequency distribution during an increase in velocity. Instead, the maximum in amplitude was due to redistribution of bed material from the bed to the freeboard and to the cyclone side.

An important application of frequency domain analysis is in validating the hydrodynamic scaling relationships with respect to the dynamics of the bed. This was done either by comparing dominant frequencies of a scaled model with those of the full-scale unit (Newby and Keairns, 1986), or by comparing the frequency spectra in a certain range of frequencies (Nicastro and Glicksman, 1984; Glicksman et al., 1993). However, extending the range of frequencies studied far beyond the range corresponding to the bubble dynamics (as was done by Glicksman et al., 1993) to include regions of low energy fluctuations, requires high accuracy of the pressure transducer used, details given on the calculations of the spectrum and a suitable representation of the spectrum (such as semi-logarithmic or logarithmic representation). If not, spectra are difficult to interpret. Most work, dealing with frequency domain analysis, identifies dominant frequencies and little information is available on the distribution of energy over a wider range of frequencies.

1.1.3. State-space analysis

Two-phase flow in fluidized bed systems is governed by non-linear relationships (equation of motion for the gas and solid phases) and, accordingly, several authors (Daw and Halow, 1991; van den Bleek and Schouten, 1993; Vander Stappen et al., 1993; Skrzycke et al., 1993; Hay et al., 1995) found time series from pressure and voidage measurements in fluidized beds to exhibit the characteristics of low-dimensional deterministic chaos. The fractal dimension in state-space was found to be of a relatively low dimension, typically less than five. Recently developed non-linearity tests applied on bubbling fluidized bed data have confirmed the data to be non-linear (Vander Stappen, 1996). However, application of non-linear time-series (state-space) analysis on experimental time series containing noise is not straightforward and the analysis methods are still a subject of research. There are investigations which found fluidized bed data to resemble noise rather than being non-linear of a low dimension. Tam and Devine (1989) discussed the problem of handling noise in measured time series from fluidized beds. When they applied state-space analysis on their data they did not observe any low-dimensional attractor. Letaief et al. (1995) investigated a low velocity bubbling fluidized bed and found it to have the characteristics of noise, similar to that of fractal Brownian motion. The two latter investigations were limited to a narrow band of operational conditions (to velocities near minimum fluidization velocity), and that may be the reason for their conclusions. Application of state-space analysis together with a non-linearity test over a wide range of fluidization regimes is lacking in literature.

All methods of non-linear time-series analysis are, in principle, based on the construction of an attractor of the dynamic evolution of the system in state-space. The method of reconstruction in state-space, known as 'embedding', is theoretically (Takens, 1981) based on the fact that all information needed to define the state of the system exists in a time series of one single measured parameter, such as the fluctuating pressure in fluidized beds. The most common methods to characterize the attractor are the evaluation of the correlation dimension and the (Kolmogorov) entropy (Grassberger and Procaccia, 1984) and/or determination of the Lyapunov exponents (e.g., Eckmann et al., 1986; Abarbanel et al., 1990). The correlation

dimension expresses the number of degrees of freedom of the system, whereas the entropy and the Lyapunov exponents are measures of the predictability of the system and the sensitivity to initial conditions. There are several text-books with descriptions of available methods for non-linear time-series analysis (Moon, 1992; Argyris et al., 1994; Hilborn, 1994; Abarbanel, 1996; Baker and Gollub, 1996). For fluidized bed systems, the correlation dimension and the (Kolmogorov) entropy have been used (Daw and Halow, 1991; van den Bleek and Schouten, 1993; Schouten et al., 1996), whereas calculation of Lyapunov exponents is associated with difficulties (Schouten et al., 1994c; Vander Stappen, 1996).

1.1.4. Comparison of frequency domain and state-space analysis

Both dynamic systems in chaotic motion and stochastic systems have a strong decay in auto-correlation function with time lag (e.g., Argyris et al., 1994) and broad-banded power spectra (e.g., Tennekes and Lumley, 1972; Abarbanel et al., 1993; Baker and Gollub, 1996). In some cases, these spectra may contain distinct peaks corresponding to some characteristic frequency of the system, such as a peak from an excitation (drive) frequency (Casdagli et al., 1992; Moon, 1992; Baker and Gollub, 1996). The link between the shape (fall-off with frequency, f) of the power spectrum and the type of system (chaotic/deterministic or stochastic) on measured time series may be used to characterize the system, since the fall-off at high frequencies is different for the two types of system. Stochastic and multifractal systems (with wide range scaling) give spectra $P(f)$, which fall-off according to a power-law of the frequency, $P(f) \sim f^{-\alpha}$ (e.g., Sigeti and Horsthemke, 1987; Tessier et al., 1993). The power spectrum of systems which exhibit deterministic chaos with a low number of modes should fall exponentially (i.e., faster than a power law) with frequency, $P(f) \sim \exp(-f/\mu)$ (Frisch and Morf, 1981; Sigeti, 1995a, 1995b). This difference in fall-off has been observed in model systems (Greenside et al., 1982; Sigeti, 1995a, 1995b), as well as on experimental time series (Brandstater and Swinney, 1987; Babloyantz and Destexhe, 1988; Philippou et al., 1991; el-Hamdi et al., 1993). Based on an investigation on various modeled time series, Sigeti (1995b) suggests that the exponential decay constant, μ, being an inverse time scale, is an invariant of the dynamics of the system and is unique to deterministic chaos. He argues that μ should be related to the positive Lyapunov exponents and found, for chaotic model equations, μ to be roughly proportional to the sum of the positive Lyapunov exponents. As a consequence of this result, the sum of the positive Lyapunov exponents (which should then be equal to the Kolmogorov entropy) of experimental systems would be possible to estimate from the power spectrum. Nowak et al. (1993), Ding and Tam (1994), Ding (1997) analyze the fall-off in power spectrum on time series measured in fluidized beds and Kikuchi et al. (1997) make a similar analysis on a three-phase reactor. The authors consider an exponential fall-off to be typical for a low-dimensional behavior, whereas a power-law fall-off is characteristic for either a stochastic process or high-dimensional chaos. They did not, however, make any quantification of the fall-off, such as comparing the decay constant with the Lyapunov exponents or entropy in line with the work of Sigeti.

The practicality of using power spectrum fall-off to quantify the entropy or distinguish low-dimensional non-linear dynamics from stochastic behavior is not resolved at present. In spite of the impression that it is generally accepted that power spectra of time-series from model systems exhibiting deterministic chaos decay exponentially (Sigeti, 1995a, 1995b), there are no systematic studies on application of this difference to *measured* time series. Such a study may

be difficult since most real systems have many modes (many degrees of freedom) and noise is present in the measurements. As for the non-linear state-space analysis, data sets with long duration and with high resolution in amplitude and time domain are needed to verify such a procedure. There also exist some examples in the literature which contradict the relevance of such a division with respect to the characteristics of the fall-off in power spectrum (Greenside, 1997). For example, Ahlers and Behringer (1978) found power-law fall-off from heat transport measurements on a Rayleigh–Bernard convection cell, a result which should not be due to stochastic effects. Furthermore, numerical integration of a deterministic partial differential equation, the Kuramoto–Sivashinksy equation, gives a solution with a power-law decay in the power spectrum, although it turns into an exponential decay at high frequencies (Manneville, 1981).

1.2. Aim and outline of paper

Two-phase flow in circulating fluidized bed (CFB) risers is complex, it depends on the operational conditions, and it may differ between different types of risers and solids used. Therefore, it is desirable to have reliable methods for an experimental mapping of the flow. Yet, these methods should be simple in order to facilitate measurements under industrial conditions (at elevated temperature and pressure). Pressure measurements are simple, reliable and possible to carry out under industrial conditions.

As indicated in the previous sections, the problem of generalization of available results lies mainly in the interpretation of measurements. There is no systematic comparison available of the outcome of different methods of time-series analysis applied on two-phase flow measurements. The present work intends to compare the different methods to evaluate pressure fluctuation measurements in a fluidized bed for characterization of the fluid-dynamics, such as identification of different fluidization regimes. Video recordings, measurements of the vertical solids concentration profile and net solids flux together with the superficial gas velocity define the operating conditions of the fluidized bed. Focus is on the data analysis rather than on the regimes, and the experimental conditions given are only examples.

A comparison is made with a time series from a well-known low-dimensional (three modes) chaotic model system (the Lorenz equations), and with a time series from measurements of velocity fluctuations in turbulent gas-flow. The Lorenz equations (Lorenz, 1963) is a simplified model of atmospheric dynamics describing (with Navier–Stokes equations) a fluid-layer under gravity, which is heated from below resulting in a temperature gradient across the layer. The result of a sufficiently large temperature gradient across the layer is that warm air rises and cool air falls. A vortex-like motion is obtained. The equations in the three dimensions x, y and z are

$$\dot{x} = \sigma(y - x)$$

$$\dot{y} = \rho x - y - xz$$

$$\dot{z} = -\beta z + xy \tag{1}$$

whose solution with $\sigma = 16$, $\rho = 45.92$ and $\beta = 4.0$, gives a chaotic time series. In this work, the x-component is chosen to exemplify the dynamics of a chaotic time series. The time series with velocity fluctuations in turbulent gas-flow in a pipe was provided by Johansson (1997). The measurements of velocity fluctuation, $\acute{u}$, in the flow direction by a hot-wire anemometer, were made in a wind-tunnel at a Reynolds number of about 60,000. Gas-phase turbulence under these conditions is normally considered as a stochastic system (many modes).

The paper is organized as follows. Section 2 describes the experimental method, and the methods of time-series analysis are briefly described in Section 3. Results and discussions are given in Section 4. Firstly (Section 4.1), the methods of data analysis are applied on four well established fluidized bed flow conditions (time- series of pressure fluctuations available at http://www.entek.chalmers.se/ ~ fijo) with significantly different flow structure (three types of bubbling regimes and a case corresponding to transport conditions). Intermittent structures of the pressure fluctuations are identified and discussed in Section 4.2. In Section 4.3, the different time-series analysis methods are used to study the fluid-dynamics as operation (in this case gas velocity) changes from non-circulating to circulating conditions. Based on the results from all time series investigated, Section 4.4 focuses on a comparison between the frequency domain and state-space analysis. The conclusions given in Section 5 are grouped into those of direct implications for description of the flow regimes studied (Section 5.1) and into more general conclusions with respect to the comparison between frequency domain and state-space analysis (Section 5.2).

2. Experiments

The experiments were carried out in a CFB-unit, shown in Fig. 1, operated under ambient conditions. The riser has a cross-section of 0.12×0.7 m and a total height of 8.5 m. The front side is made of transparent perspex to facilitate visual observations and video recordings. The air distributor was a perforated plate with 2 mm holes and 6.2% hole area having a pressure drop similar to that of CFB boilers. To prevent particles from falling down through the plate into the wind-box, the plate was covered with a fine-mesh net. For comparison, some runs at low velocities were made with a high pressure-drop air distributor. Then the bottom side of the air distributor was partly blocked by tape, resulting in about 0.4% free hole area. The bed material was silica sand with an average particle size of 0.31 mm and a particle density of 2600 kg/m^3, i.e., Group B particles. The particle size distribution is shown in Fig. 2.

A pneumatically controlled butterfly valve in the down-comer, from the cyclone, measures the net solids flux, G_s. The valve plate is perforated and covered with a fine mesh net. When the valve is closed, it acts as an air distributor on which a bubbling bed is formed. During the closure of the valve, the pressure drop over the bubbling bed is recorded with a transducer connected to two pressure taps, p_1 and p_2, as indicated in Fig. 1. The solids flux, G_s can be calculated as

$$G_s = \frac{1}{g}\frac{\mathrm{d}p}{\mathrm{d}t}\frac{A_d}{A} \tag{2}$$

where $\mathrm{d}p/\mathrm{d}t$ is the slope of a line fitted (least square method) to the recorded pressure-drop

data. A and A_d are the cross-section areas of the bed/riser and the cyclone down-comer. The pressure transducers for the pressure drop measurements and for the solids flux measurement were recorded by an AD converter connected to a PC.

For qualitative interpretation of the fluidization regimes of the bottom bed and the splash zone, video recordings were made with a Super VHS video system with a recording speed of 25 frames/s. A camera shutter speed (adjustable) of 1/250 of a second was sufficient to get distinct single frame pictures.

Two sets of pressure measurements were carried out: pressure drop to determine the axial solids concentration profile and pressure fluctuations for the time-series analysis.

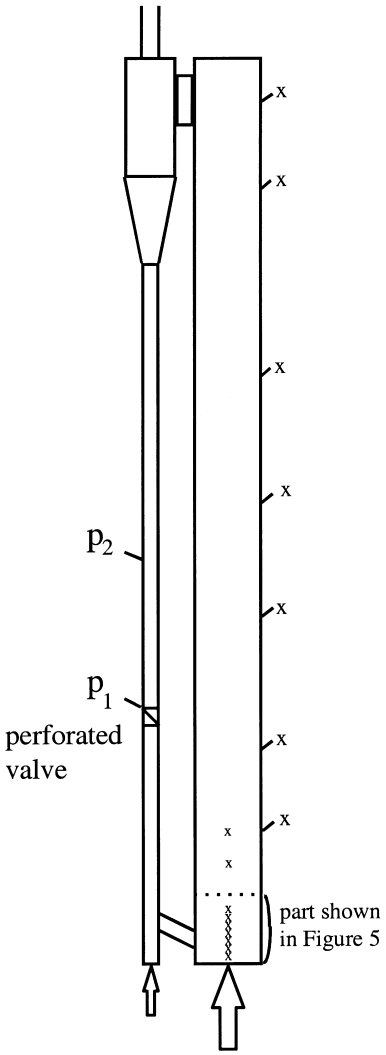

Fig. 1. The cold CFB unit. The riser is 8.5 m tall and have a 0.70 × 0.12 m cross-section. Two air distributors with different pressure drop were used. The pressure taps are indicated by x and the two pressure taps for solids flux

Pressure drop. Piezo-resistive pressure transducers were connected to pressure taps along the riser height and the sampling frequency was 20 Hz during 5 min. To detect the strong gradient in solids concentration in the lower part of the riser the taps are densely spaced in this region. Pressure drop due to hold-up of the gas, frictional and acceleration effects of gas and particles is neglected. Although the pressure drop due to acceleration of the bed particles ($= G_s(u - u_t)$, u is the superficial gas velocity and u_t is the terminal velocity) may give a significant contribution to the measured pressure drop at high circulation rates, G_s, it can be neglected under the present (boiler) conditions for which G_s is less than 25 kg/m^2 s (Johnsson and Leckner, 1995).

Pressure fluctuations. The pressure fluctuations were recorded as gauge (single ended) pressure through a 50 and 4 mm I.D. steel tube with a fine mesh net at the side facing of the fluidized bed. The transducer (Kistler Type 7261) has a response frequency greater than 1 kHz and an adjustable range (charge amplifier Type 5011A10) giving the optimum response for each condition. The charge amplifier acts as a high-pass filter with a filter frequency of 0.1 Hz and only the fluctuating part of the signal was recorded. van Ommen et al. (1999) showed that a model by Bergh and Tijdeman (1965) give good predictions for this type of transducer and probe systems. The model predicts the first resonance frequency to be 670 Hz and the amplitude ratio at 200 Hz (Nyquist frequency in the present work) to be 1.11 and lower at lower frequencies (e.g., 1.03 at 100 Hz). Thus, the results indicate that no significant distortion of the signal can be expected in the range of frequencies studied. The pressure transducer was connected to a 16 bit data acquisition board (Difa ABP 200). The data recorded were stored on a PC. The signals were low-pass (hardware) filtered at the Nyquist frequency. The sampling frequency was 400 Hz for all fluctuating signals and 786,432 samples were taken, corresponding to 33 min of total sampling time.

The CFB was operated with a constant total inventory of solids and with gas velocities ranging from 0.6 to 5 m/s. As the velocity is increased, solids are transferred from the bottom

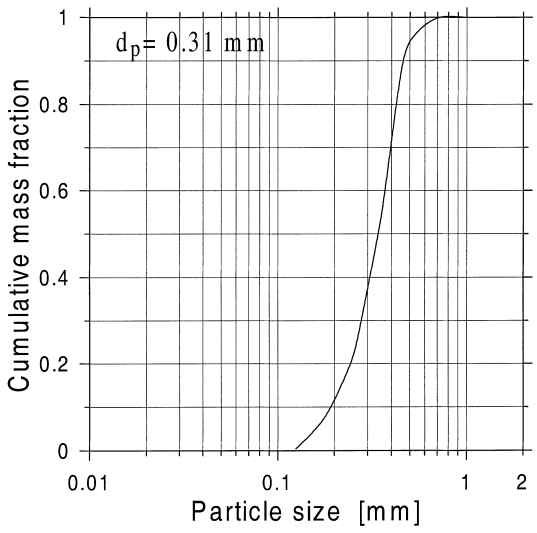

Fig. 2. Particle size distribution of the solids.

bed to the splash- and transport zones resulting in a decrease in height of the bottom bed. In most cases the in-bed measurements, which were taken at 0.2 m above the air distributor, were within the bottom bed and high enough from the bottom of the bed not to be influenced by entrance effects from the air distributor. The bottom bed height, H_x, is defined as the part of the pressure drop which falls on a straight line (Fig. 6), and not as the extrapolated bed height, a method for determination of the bed height which is not valid at high velocities.

3. Time-series analysis

All analysis are made on time-series with data points $x(n)$, with $n = 1,2,3,\ldots,N$, measured at equidistant time intervals, Δt, i.e., with a sampling frequency of $f_s = 1/\Delta t$. N is the total number of samples and x is the pressure signal. There are numerous text books which provide details on time and frequency domain analysis, e.g., Bendat and Piersol (1971), Rabiner and Gold (1975), Proakis and Manolakis (1989), Press et al. (1992). These methods are also used for statistical description of turbulence (see Tennekes and Lumley, 1972).

3.1. Time domain analysis

The amplitude of the signal, x, is expressed by the standard deviation (square root of second-order statistical moment):

$$\sigma = \sqrt{\frac{1}{N-1}\sum_{n-1}^{N}(x(n)-\bar{x})^2}, \tag{3}$$

with the average,

$$\bar{x} = \frac{1}{N}\sum_{n=1}^{N}x(n). \tag{4}$$

The higher order statistical moments are expressed in a non-dimensional form (Tennekes and Lumley, 1972) as the skewness (normalized third-order statistical moment)

$$S = \frac{1}{N\sigma^3}\sum_{n=1}^{N}(x(n)-\bar{x})^3 \tag{5}$$

and the flatness (normalized fourth-order statistical moment)

$$F = \frac{1}{N\sigma^4}\sum_{n=1}^{N}(x(n)-\bar{x})^4. \tag{6}$$

The skewness, the lack of symmetry in the probability distribution, is zero for a normal distribution. The flatness is a measure of the sharpness of the distribution. It is 3 for normal,

Gaussian distribution. For intermittent systems, the flatness can also be seen as the ratio of the time spent under quiescent conditions to the time spent under active conditions.

The correlation between two points separated by a time lag, k times Δt, is expressed with the auto-correlation function

$$c_{xx}(k) = \sum_{n=0}^{N-|k|-1} (x(n) - \bar{x})(x(n-k) - \bar{x}) \tag{7}$$

which, normalized with the value at zero lag, $c_{xx}(0)$, becomes

$$C_{xx}(k) = \frac{c_{xx}(k)}{c_{xx}(0)}, \tag{8}$$

i.e., $-1 \leq C_{xx} \leq 1$.

3.2. Frequency domain analysis

In fluidized beds, the major frequency content of pressure fluctuations is normally below 10 Hz. Thus, to determine dominant frequencies, sampling with 20 Hz is sufficient. For a power spectrum with a frequency resolution of 0.05 Hz, 400 samples are required. This corresponds to a sampling time of 20 s, which, however, is far too short to describe the spectrum with a sufficient statistical significance. The variance of such an estimation of the power spectrum is large, of the order of the square of the power spectral density, and will not decrease with an increased number of samples. This is the case, because a single power spectrum can be seen as one sample in the frequency domain. In order to decrease the variance, the power spectrum is estimated as an average of a number of sub-spectra, the number chosen to get a satisfactory trade off between frequency resolution and variance. Hence, the time series is divided into L segments of individual length N_s which are represented as

$$x_i(n) = x(n + iN_s) \quad n = 1,2,\ldots,N_s, \quad i = 1,2,\ldots,L \tag{9}$$

The power-spectrum estimate of each segment is

$$P^i_{xx}(f) = \frac{1}{N_s U} \left| \sum_{n=1}^{N_s} x_i(n) w(n) \exp(-j2\pi f n) \right|^2, \tag{10}$$

where U normalizes by a factor of the power in the window function, $w(n)$. Thus,

$$U = \frac{1}{N_s} \sum_{n=1}^{N_s} w^2(n). \tag{11}$$

The averaged power spectrum becomes

$$P_{xx}(f) = \frac{1}{L} \sum_{i=1}^{L} P^i_{xx}(f). \tag{12}$$

Eqs. (9)–(12) comprise the Welch method of power spectrum estimation (Welch, 1967) without overlap between data segments. The frequency resolution of the power spectrum is $\Delta f = f_s/N_s$. The decrease in variance of the power spectrum is approximately proportional to the number of spectra averaged (Bendat and Piersol, 1971), $\sim L^{-1}$. A Hanning window is used as window function, $w(n)$ (see, e.g., Press et al., 1992). This window is a smooth one with a continuous first derivative, and both the window and its derivative are zero at the endpoints. This is of importance when studying the characteristics of the spectrum at high frequencies, since when the time series is multiplied by the window, the resulting series must be continuously differentiable (Sigeti, 1995b, 1996).

In accordance with Parseval's theorem, the energy of the signal is conserved in the frequency domain,

$$E_x = \frac{1}{N}\sum_{n=1}^{N}|x(n)|^2 \approx \frac{1}{N_f}\sum_{k=1}^{N_f}P_{xx}(f), \tag{13}$$

where $N_f = f_N/\Delta f$. Thus, the energy of the signal, E_x, which lies in a given frequency range is obtained from summation of the power spectrum over the frequency range of interest.

Here, all sub-spectra are based on 8192 samples ($\approx$20 s) yielding an average of 96 spectra. With the 400 Hz sampling frequency, this gives power spectra with a frequency resolution of 0.048 Hz. As discussed above, this sampling frequency is far higher than what is needed ($\sim$20 Hz) to resolve the major range of frequencies in fluidized beds.

3.3. State-space analysis

The theory of non-linear time series (chaos) analysis is still subject to research, and different algorithms and methods are available in literature. Most of the methods are based on the principle of reconstruction of the data into an attractor in state-space. Details of the analysis applied are given by van den Bleek and Schouten (1993) and Schouten et al. (1994a), (1994b) and only a brief description is given here.

The reconstruction of the data into an attractor in state-space is based on the method developed by Takens (1981). The reconstructed attractor, which, according to the theorem of Takens, has the same properties as the true attractor, is described by two invariants, the Kolmogorov entropy and the correlation dimension. Fig. 3 is a schematic illustration of a two-dimensional reconstruction of an attractor. The reconstructed attractor consists of orbits of points corresponding to different state vectors, $\bar{X}(i)$, Fig. 3b. A state vector represents one point on the orbit of the attractor and is reconstructed from the data points of the time series, Fig. 3a. It is obtained by choosing a specific time delay, τ, of equal sequential time steps between the elements of the state vector and the number of elements, m, of the state vector. Thus, as an example $\tau = 1$ and $m = 3$ give the state vectors, $\bar{X}(1) = (x(1),x(2),x(3))^{\mathrm{T}}$, $\bar{X}(2) = (x(2),x(3),x(4))^{\mathrm{T}}$, $\bar{X}(3) = (x(3),x(4),x(5))^{\mathrm{T}}$, etc. In Fig. 3, $m = 2$ and the time delay is equal to the time between the samples, i.e., $\tau = 1$ (corresponding to $1/f_s$). In general, the reconstructed state vector is

$$\bar{X}(i) = \big(x(i),x(i+\tau),x(i+2\tau),\ldots,x(i+(m-1)\tau)\big)^{\mathrm{T}}. \tag{14}$$

The number of elements of the state vector, m, which equals the number of coordinates in state-space, is called embedding dimension. If there is no delay (no data points skipped) between successive vector elements, τ is one (as in Fig. 3). T is the time window, i.e., the length of the reconstructed vector, $\bar{X}(i)$, measured in units of time. This time window is a segment $[t,t+T]$ of the time series with length $T = m\tau\Delta t$. There are no strict rules on the choice of the embedding dimension, m, (e.g., Provenzale et al., 1994; Vander Stappen, 1996). Here, it is calculated as the number of data points, N, divided by the number of cycles, i.e., $m = N/N_c$. The number of cycles, N_c, is the number of times that the time series crosses its average value, $\bar{x}$, divided by two. Thus, related to m, the average cycle frequency (the number of times per time unit the signal crosses its average) is defined as

$$f_c = \frac{N_c}{N\Delta t}. \tag{15}$$

From practical experience (Vander Stappen, 1996; Schouten et al., 1994a) m should be in the order of 50–200 points per cycle, which for a fluidized bed system, results (for $\tau = 1$) in sampling frequencies of 50–200 times the cycle frequency, since $f_s = m/T$. This, of course, also determines the requirements on the response time of the measurement device, i.e., for pressure measurements in a fluidized bed, the total response time of a pressure tap with tubing, pressure transducer and AD converter should at least be less than 20 ms.

A strictly periodic time series has an average cycle frequency, which is identical to the peak frequency of its power spectrum. Since the peak frequency in a power spectrum is sometimes used to characterize the dynamics of fluidization (e.g., 'dominant bed frequency', 'fundamental

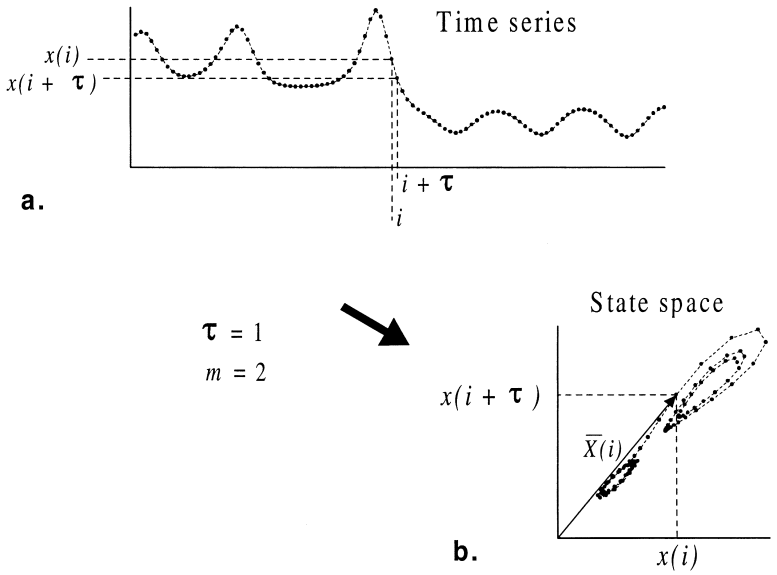

Fig. 3. A schematic illustration of a two-dimensional reconstruction of an attractor: (a) time series, $x(i)$; (b) two-dimensional state-space. The reconstructed attractor consists of orbits of points corresponding of different state vectors, $\bar{X}(i)$, Fig. 3b.

frequency of bed fluctuations') a comparison between this frequency and f_c is of interest. A considerable difference between these two frequencies is a first indication that the peak frequency alone is not representative for the dynamics of the signal, because then the signal contains a considerable amount of energies at other frequencies than the peak frequency.

Since a state vector represents one point on the orbit of the attractor, the complete set of state vectors constitutes a set of points on the orbits of the attractor in state-space. From these, a corresponding set of distances between all pairs of points of neighboring orbits of the attractor can then be derived. The dimension and entropy of the attractor are determined from this set of distances.

3.3.1. Correlation dimension

A maximum likelihood estimation of the correlation dimension, D_{ML}, is used to describe the spatial complexity of the attractor in state-space. It is estimated from the distribution of distances between points on the attractor. A detailed description is given by Schouten et al. (1994a). For a chaotic system, the attractor is called a strange attractor and it may have a non-integer value of D_{ML}.

The method used to calculate D_{ML} is based on the correlation integral given by Grassberger and Procaccia (1983a, 1983b)

$$C(l) = \frac{1}{N(N-1)} \sum_{i \neq j} \Theta\big(l - \|\bar{X}(i) - \bar{X}(j)\|\big), \tag{16}$$

where Θ is the Heaviside function. The correlation integral expresses the probability of finding pairs of points $(\bar{X}(i), \bar{X}(j))$ on the attractor within the specific distance, l. With D as the correlation dimension, the correlation integral scales as $C(l) \approx l^D$ when $l \to 0$ and $N \to \infty$. There are several ways of estimating the correlation dimension from the correlation integral. Here, it is obtained by applying the maximum likelihood estimation by Takens (1985). Thus, the dimension estimate becomes

$$D_{ML} = \left[\frac{1}{M} \sum_{i=1}^{M} - \ln(r_i) \right]^{-1} \tag{17}$$

where M is the sample size of interpoint normalized distances $r_i = l_i / l_0$. The distances, l_i, are normalized with respect to a maximum scaling distance, l_0, which is taken (Schouten et al., 1994a) as the average absolute deviation

$$\mathrm{AAD} = \frac{1}{N} \sum_{n=1}^{N} |x(n) - \bar{x}|, \tag{18}$$

a measure similar to the standard deviation in Eq. (3)).

3.3.2. Kolmogorov entropy

The Kolmogorov entropy, K, is a measure of the loss of information along the attractor. It is defined from information theory (Grassberger, 1986), which states that the information

needed to predict a system during the time interval $[t_1, t_2]$, given the information $I_{[t_1]}$ in bits at time t_1, is

$$I_{[t_1,\,t_2]} = I[t_1] + K(t_2 - t_1) \tag{19}$$

for $K(t_2 - t_1) \rightarrow \infty$. Hence, for a fully predictable system $K = 0$ and for a stochastic system K is infinity. For a chaotic system, K is finite and positive. K can also be calculated by the maximum likelihood method as described by Schouten et al. (1994b). For a measured time series reconstructed into state-space, the separation of nearby points on different orbits on the attractor is assumed to be exponential (Grassberger and Procaccia, 1983a, 1983b, and the separation can be expressed as an exponential distribution

$$C(b) = \exp(-Kb/f_s) \quad b = 1,2,3,\ldots. \tag{20}$$

The variable b is the number of sequential pairs of points on the attractor for which the distance exceeds some maximum interpoint distance, l_0. The maximum likelihood estimation of the entropy, K_{ML}, becomes (Schouten et al., 1994b)

$$K_{ML} = -f_s \ln\left[1 - \frac{1}{\bar{b}}\right] \tag{21}$$

with

$$\bar{b} = \frac{1}{M}\sum_{i=1}^{M} b_i. \tag{22}$$

The Kolmogorov entropy may be expressed in bits/cycle, in bits/time-unit (e.g., bits/s), or, in numerical works, in bits/iteration (not considered here). In bits/cycle, it expresses the amount of information lost under an average cycle $(1/f_c)$ in the time series, corresponding to an average orbital period on the attractor. If K_{ML} is related to the average cycle time (seconds), it is expressed in bits/s and then reflects the infomation lost in 'real' time units. Thus, two systems of different time-scale may have the same entropy per cycle.

3.3.3. Non-linearity test

Not only low-dimensional chaos will generate finite dimensions but this could also result from different sorts of stochastic processes with long time correlation and power-law power spectra, such as fractal Brownian motion (Provenzale et al., 1994 and references therein). In addition to the non-linear analysis, we must therefore investigate if the time series is non-linear. Various tests have been developed for this purpose (Kennel and Isabelle, 1992; Takens, 1993; Provenzale et al., 1994 and references therein). The tests are based on creating a surrogate data series with the same power spectrum as the original signal but with no phase correlation. This can be done by substituting the Fourier phases of the measured time series with random and uniformly distributed phases. The surrogate time series, which yields the same power spectrum, autocorrelation and statistics as the original time series, is obtained by inverting the phase randomized Fourier spectrum. If the signal is non-linear, this procedure will change the outcome of a non-linear analysis, such as the estimation of the correlation

dimension described above. If, on the contrary, there is no difference in the outcome when applied on the surrogate time series, the time series cannot be shown to be non-linear or chaotic. Often, the outcome of the test is compared with a null hypotheses, i.e., the null hypotheses is rejected if the outcome of the non-linear analysis is significantly different from the original time series. Normally, the difference between the original time series and the surrogate time series is expressed in number of standard deviations of the surrogate series, called the Z-value.

The method used here is described by Schouten (1997). It is a combination of the methods given by Kennel and Isabelle (1992) and Takens (1993). The test compares the original and surrogate time series with respect to their short-time predictability in state-space. The discriminating statistics for the test is similar to the concept of Kolmogorov entropy as described above and by Schouten et al. (1994b). The surrogate time series has the same Fourier spectrum and noise as the original time series. Here, a Z_{avg} value is reported which has to be less than -3 to reject the null hypotheses at a 99% confidence interval (Schouten, 1997). Hence, the lower the value of Z_{avg} the higher the significance of rejecting the time series as being generated by a linear stochastic process.

4. Results and discussion

The pressure drops of the air distributor and fluidization velocities employed in the present work cover three bubbling regimes (cf. Svensson et al., 1996a). At velocities higher than the transport velocity, u_{tr}, the riser is operated under transport conditions. Here, u_{tr} is defined as the velocity above which there is no bottom bed, and all solids introduced to the riser are transported in entrained flow (except for some solids present in an acceleration one just above the air distributor). The transport velocity depends on the configuration and operation of the system and on the amount and type of solids in the CFB-loop. At velocities lower than u_{tr}, the unit was operated in the multiple, single and exploding bubble regimes. The multiple and single bubble regimes are limited to non-circulating conditions (the net solids flux $G_{\mathrm{s}} = 0$), whereas the exploding bubble regime can occur under non-circulating as well as circulating conditions (Svensson et al., 1996b; Zijerveld et al., 1998). Under the present test conditions u_{tr} is about 4 m/s, and the transport conditions are associated with a solids flux, G_{s}, which typically exceeds 20 kg/m^2 s. The range of operation is summarized in Fig. 4.

4.1. Four different flow conditions

The focus is on the flow in the bottom region of the riser. Under non-circulating conditions all solids are, of course, located in this region, but also under circulating conditions and velocities lower than u_{tr} the major part of the solids in the riser is found in the bottom bed. Only for velocities exceeding u_{tr}, the solids concentration is fairly even and only slightly higher in the lower section than in the upper part of the riser. Four conditions, two non-circulating and two circulating are treated: the multiple bubble and the single bubble regimes, both at a gas velocity of 0.6 m/s, the exploding bubble regime at 2.2 m/s at a low solids flux under

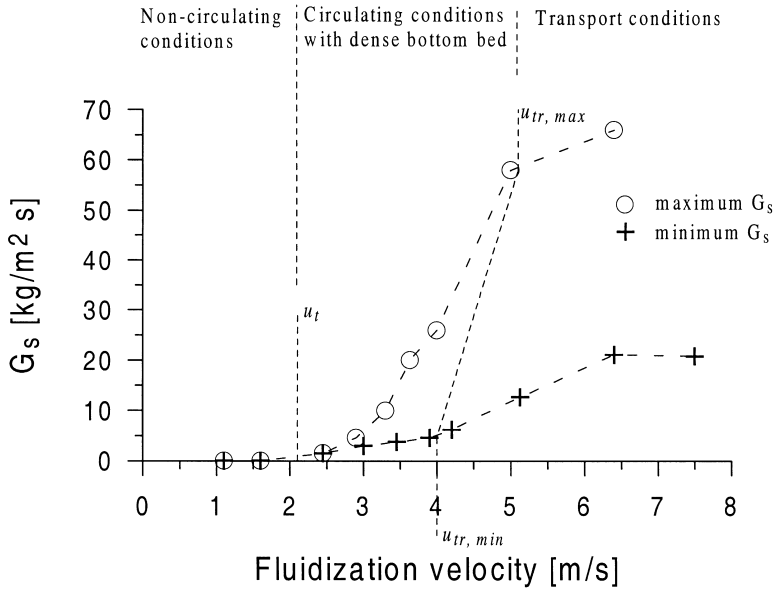

Fig. 4. Solids fluxes, G_s, vs. velocity in the CFB unit of Fig. 1. The maximum and minimum solids fluxes were obtained by control of the purge air to the inlet of the recycled solids. The terminal velocity of an average size bed particle, u_t, and the transport velocity, u_{tr}, are indicated.

circulating conditions ($G_s \sim 1$ kg/m^2 s, cf. Fig. 4), and transport conditions at 4.1 m/s ($G_s = 25$ kg/m^2 s).

4.1.1. A qualitative picture of the flow

The video frames of Fig. 5 give a qualitative picture of the bottom-bed flow in the four cases. The three bubbling regimes have similar bed heights but show strong differences in the bubble behavior (Fig. 5a–c). The multiple bubble regime (Fig. 5a) occurs at low velocities and a high air distributor pressure drop ($u = 0.6$ m/s, $\Delta p_d = 4200$ Pa shown in the figure), and is a well fluidized bubbling bed; a 'normal' bubbling bed with a uniform bubble distribution. There is a continuous passage of bubbles through the bed, in Fig. 5a, and several bubbles erupt simultaneously at the surface of the bed. The pressure drop across the air distributor, Δp_d, is of the same order as the pressure drop across the bed, Δp_x. The bubbles are much smaller than the wide bed dimension (0.7 m) and a considerable number of bubbles are also smaller than the narrow bed dimension (0.12 m). Therefore, more bubbles erupt at the surface of the bed than seen from the front of the bed. The gas flow through the bed appears to be constant in time with the bubbles evenly distributed over the cross-section of the bed (Svensson et al., 1996a).

Fig. 5b shows a bubble just before eruption, when the bed is operated in the single bubble regime ($u = 0.6$ m/s, $\Delta p_d = 660$ Pa). The pressure drop across the air distributor is considerably lower than the pressure drop across the bed, but fulfills some published criteria for the minimum ratio of $\Delta p_d/\Delta p_x$ needed for an even fluidization (e.g., Qureshi and Creasy, 1979), but is too low with respect to other criteria (e.g. Zuiderweg, 1967). The video recording shows an even fluidization in terms of symmetry; on a time average basis the center of the bubbles

coincides with the center-line of the bed. However, there is a strong interaction with the wind-box (Svensson et al., 1996a) and obviously the gas flow cannot be continuous, since, after the eruption of a bubble, the bed collapses to a state free of bubbles, lasting for a short time, during which the velocity is not higher than at minimum fluidization. The latter can be concluded from a comparison of the height of the collapsed bed, obtained from the video recording, with the height of the static bed.

Large exploding bubbles occur (Fig. 5c) at a high gas velocity (but lower than u_{tr}) under circulating conditions ($u = 2.2$ m/s, $\Delta p_x = 3300$ Pa) with the same air distributor that gave the single bubble regime at low velocities. Since the maximum bubble size is limited by the bed height, these bubbles are similar in size to those of the single bubble regime and the average voidage is not much higher than for the single bubble regime. Therefore, there is a substantial through-flow of gas through the bubbles (cf. Johnsson et al., 1991) with high local gas velocities as the bubbles explode at the surface of the bed. After an eruption of the bubble, the bed collapses like in the single bubble regime. In the exploding bubble regime, there is a substantial amount of solids in the splash zone in the form of clustered particles. These particle agglomerates, are projected into the freeboard by the eruption of the bubbles and constitute the main phase of the splash zone. A distinct bed surface is seen also at this high velocity, which exceeds the terminal velocity of an average-size bed particle. Pronounced clustering leads to a strong back-mixing in the splash zone.

Fig. 5d shows the lower bed section at a velocity ($u = 4.1$ m/s) above u_{tr}. Due to acceleration effects, clustering phenomena and wall-layer back-mixing, there is a small dense region above the air distributor also at velocities above u_{tr}. The flow is characterized by clustered particles in

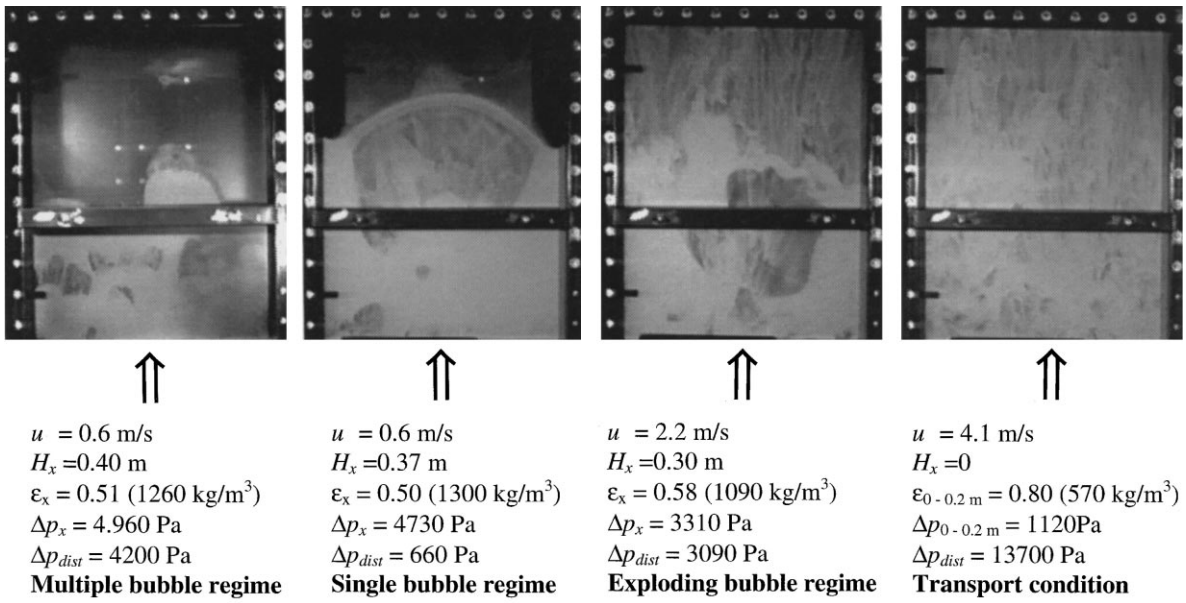

Fig. 5. Frames from video recordings of the lower part of the CFB operated in (a) the multiple bubble regime, (b) the single bubble regime, (c) the exploding bubble regime, and (d) under transport conditions. The dark horizontal part crossing the bed is a support beam for the perspex to withstand the forces from the bed-fluctuations.

strands, which are uniformly distributed over the cross-section of the riser. The average voidage is considerably lower than under the bubbling conditions.

In summary, on a macro-scale, we observe two types of flow conditions: a discontinuous and a continuous flow. In this sense, the single bubble and the exploding bubble regimes can be characterized by a discontinuous gas flow in time and space. The flow characteristics of the multiple bubble regime and the transport conditions are more continuous in nature with many small bubbles (multiple bubble regime) or strands (transport conditions) in a uniform distribution over the bed width, and the gas flow is, on a macro-scale, continuous in time and space (see also Svensson et al., 1996a).

4.1.2. Time averaged data

Table 1 summarizes the time averaged data of the four cases. The large difference in flow behavior of the multiple and single bubble regimes (Fig. 5a and b) is not seen in the time-averaged pressure drop, Fig. 6. Thus, the average solids concentration, ρ, or voidage, ε, Table 1, is similar in these two cases ($\rho \approx 1300$ kg/m^3, $\varepsilon \approx 0.5$). The similarity of the pressure profiles of Fig. 6 supports the prediction by the correlation of Qureshi and Creasy (1979) that the $\Delta p_d/\Delta p_x$-ratio was sufficient for the bed to be completely fluidized. The difference in bed height, H_x, (the dense bed is defined as the part of the pressure drop which falls on a straight line in Fig. 6) is small. The multiple bubble regime gives somewhat higher values of H_x ($=0.40$ m) and bed voidage ε ($=0.51$) than the single bubble regime ($H_x = 0.37$ m, $\varepsilon = 0.50$). This is expected, since smaller bubbles eject less solids into the splash zone and have a lower velocity than the larger bubbles of the single bubble regime.

In the exploding bubble regime, the height, H_x, of the dense bed is about 0.3 m due to transfer of solids from the bed to the splash and transport zones and to the cyclone side. The average bed voidage is $\varepsilon \approx 0.58$ and, thus, only slightly higher than in the two low-velocity cases. The pressure profile shows a considerable amount of solids above the dense bed.

Under transport conditions, there is, except for the lowest 0.2 m, a more or less constant decay in pressure over the entire riser height which yields only a weak decay in solids concentration with height. The small bottom zone is not easily determined from the pressure drop measurements. Furthermore, the high measured voidage (~ 0.8) in combination with the high solids recirculation (~ 25 kg/m^2 s) may result in a substantial contribution from

Table 1
Time averaged data for different regimes. The Reynolds number is based on the bubble diameter, or typical distance between strands in the case of transport conditions as obtained from the video recordings (cf. Fig. 5)

Regime condition	u (m/s)	Δp (Pa)	Bottom bed			
			H_x (m)	Δp_x (Pa)	ε	Re_{D_b}
Multiple bubble	0.6	5200	0.40	4960	0.51	4000
Single bubble	0.6	5340	0.37	4730	0.50	20,000
Exploding bubble	2.2	5445	0.3	3310	0.58	60,000
Tranport condition	4.1	3360	0	–	–	30,000

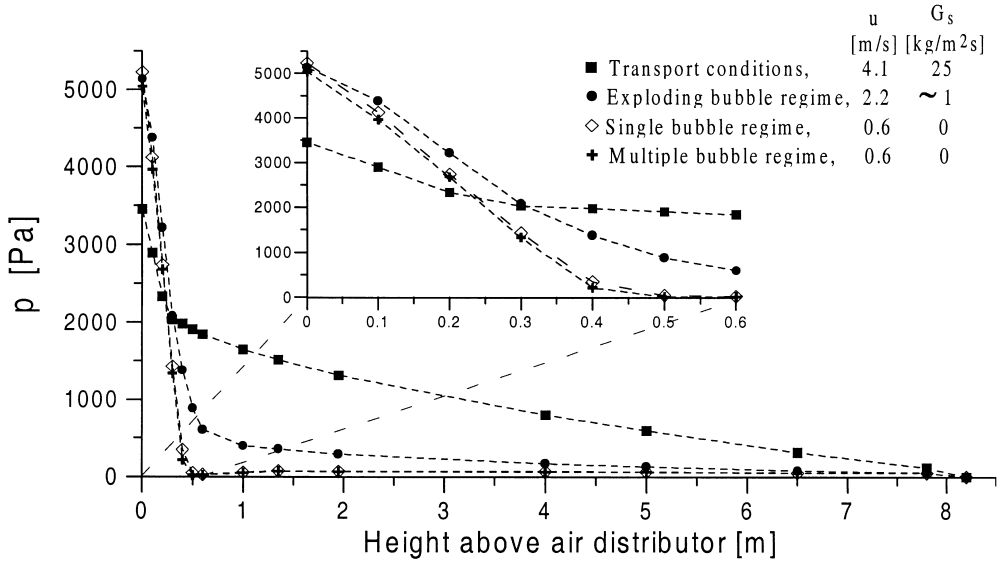

Fig. 6. The pressure distribution in the riser, operated under the conditions shown in Fig. 5.

acceleration effects to the pressure drop and, consequently, the actual average voidage may be even higher than 0.8 in the lowest section.

Except for the obvious fact that the pressure drop represents the distribution of solids in the riser (Fig. 6), we cannot draw many conclusions on differences in regimes from the pressure drop profiles.

4.1.3. Time domain analysis

The flow patterns in the single and multiple bubble regimes can be seen from in-bed pressure signals measured at 0.2 m above the air distributor, Fig. 7. There are differences both in the amplitude (standard deviation, σ, Eq. (3)) and in the time behavior of the two signals. Table 2 summarizes the outcome of the time-series analysis. The multiple bubble regime has a lower amplitude due to the smaller bubbles, $\sigma = 272$ Pa, than the single bubble regime, $\sigma = 540$ Pa. The periodicity of the signal in the single bubble regime is not present in the multiple bubble regime. The peak values of the fluctuations in the single bubble regime is about 2 kPa increasing to 4 kPa in a 1.1 m/s — case not shown. This is of the same order as the time-average total pressure drop over the bed (5 kPa, Fig. 6, Table 1), i.e., the large single bubbles lift a major part of the bed mass above the location of the pressure tap, an effect confirmed by the video recordings (see also Fig. 5a). In this sense, the single bubble regime resembles a slugging regime. Fig. 7c shows that the in-bed pressure fluctuations of the exploding bubbles have an amplitude, $\sigma = 1690$ Pa, which is greater than that of the single bubbles. The exploding bubble regime is also governed by the dynamics of large bubbles, but the signal is more complex than that of the single bubble regime, and no clear periodicity can be observed. Under transport conditions, Fig. 7d, the signal remains complex, and, since there is no dense bottom bed and less amount of solids in the riser, the amplitude is lower ($\sigma = 118$ Pa) than in the bubbling cases. It is difficult to draw any conclusions from the amplitude as such, unless

one studies its changes during the variation of some operational parameter over a wide range, such as σ vs. velocity (see Section 4.3).

The skewness, S (Eq. (5)), and flatness, F (Eq. (6)), exhibit small deviations from the values corresponding to a normal Gaussian distribution, $S = 0$ and $F = 3$, Table 2. Details in the deviations can be seen from a normal probability plot, Fig. 8, in which a straight line represents a Gaussian distribution and the curvature of deviations is emphasized by the logarithmic scale. Fig. 8 shows that all time series studied follow a Gaussian distribution within a certain range around the average value of the time series. The chaotic Lorenz system is almost symmetric ($S \approx 0$) but flatter ($F < 3$) than a Gaussian distribution. The latter result can be understood, since a substantial amount of the fluctuations of the Lorenz system does not cross the average value of the time series (cf. Fig. 13a). The velocity fluctuations of the turbulent pipe flow give, as expected (e.g., Frisch and Morf, 1981), a flatness of $F = 2.98$ which is near that of Gaussian noise ($F = 3$), Table 2 and Fig. 8e. When there is a deviation from a Gaussian distribution it occurs at frequencies above the major frequencies, with the major frequencies roughly corresponding to fluctuations with amplitudes large enough to cross the average of the time series. It is, therefore, expected that the deviation mainly occurs at frequencies of the order of or higher than the average cycle frequency, f_c, and this region needs to be studied in more detail.

Fig. 9a–d give the autocorrelation functions (Eqs. (7) and (8)), the resemblance of the signal with itself, in the four cases. As expected, there is a fast decay in autocorrelation with time-lag for the multiple bubble regime and for transport conditions (Fig. 9a and d), whereas the large bubble systems, single and exploding bubble regimes, have a more periodic autocorrelation on

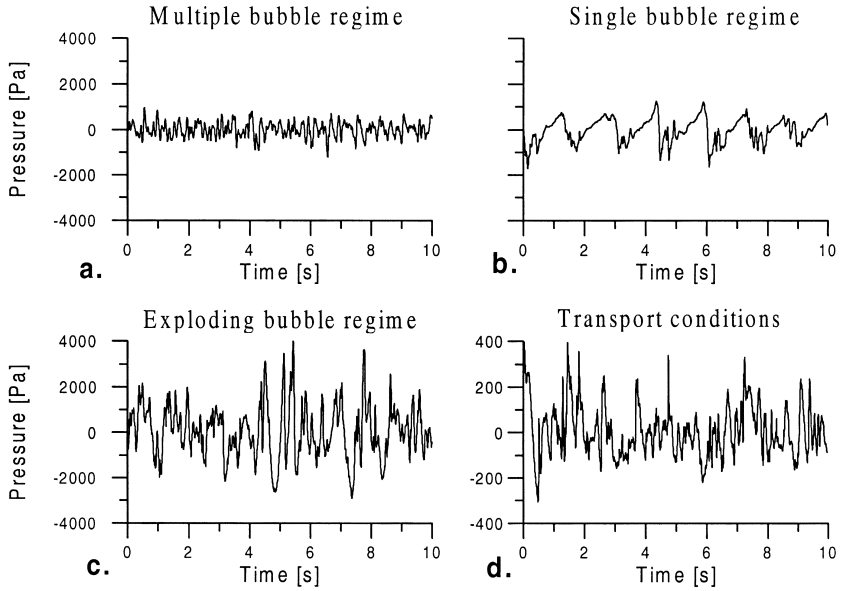

Fig. 7. Time sequences of the pressure fluctuations measured in (a) the multiple bubble regime, (b) the single bubble regime, (c) the exploding bubble regime, and (d) under transport conditions (different scale on vertical axis). The measurements were made 0.2 m above the air distributor. Operating conditions according to Table 1.

Table 2
Measures calculated by linear and non-linar analyses. Values in brackets cannot be compared with the corresponding ones of the fluidized bed data, since they were obtained for a different time scale/system. In positions marked (–), the value does not exist or has no sense in relation to the other time series. The values of fall-off are from least square power-law (power, α) and exponential (exp, $1/\mu$) fits to the spectra. The frequency-ranges of the fall-off (4–10 and 20–100 Hz) were only used for the fludized bed data. For the Lorenz model, the whole range of frequencies was used and the ranges related to the turbulent pipe-flow were determened accordidng to Fig. 12. The uncertainty of the values given is lower than 5%

	Time domain				Frequency domain					State-space			
System/regime	σ (Pa)	S	F	f_c (Hz)	f_d (Hz)	Type of fall-off 4–10 Hz	Fall-off			Z_{avg}	D_{ML}	K_{ML} (bits/cycle)	K_{ML} (bits/s)
							$1/\mu$ 4–10 Hz	α 4–10 Hz	α 20–100 Hz				
Multiple bubble	272	0.0179	3.36	5.60	2.10	exponential or power	0.283	1.86	5.40	−1.4	6.23	6.24	34.9
Single bubble	540	−0.326	3.41	1.53	0.68	exponential or power	0.323	2.17	5.10	−16.5	2.55	5.50	8.40
Exploding bubble	1690	0.586	2.92	2.64	1.25	exponential or power	0.439	2.94	4.24	−2.7	5.87	6.53	17.2
Transport	118	1.03	4.50	4.00	0.98	exponential or power	0.312	2.08	4.04	−2.5	6.16	5.70	22.8
Lorenz eqns, $x(t)$	–	0.046	2.17	(0.488)	–	exponential	1.23 entire range	–	–	−13.7	2.08	4.99	(2.44)
Turbulent pipe flow, $\dot{u}(t)$	–	−0.232	2.98	(−56.0)	–	power	–	1.64 20–100 Hz	5.90 400–2000 Hz	−0.39	8.01	5.61	(314)

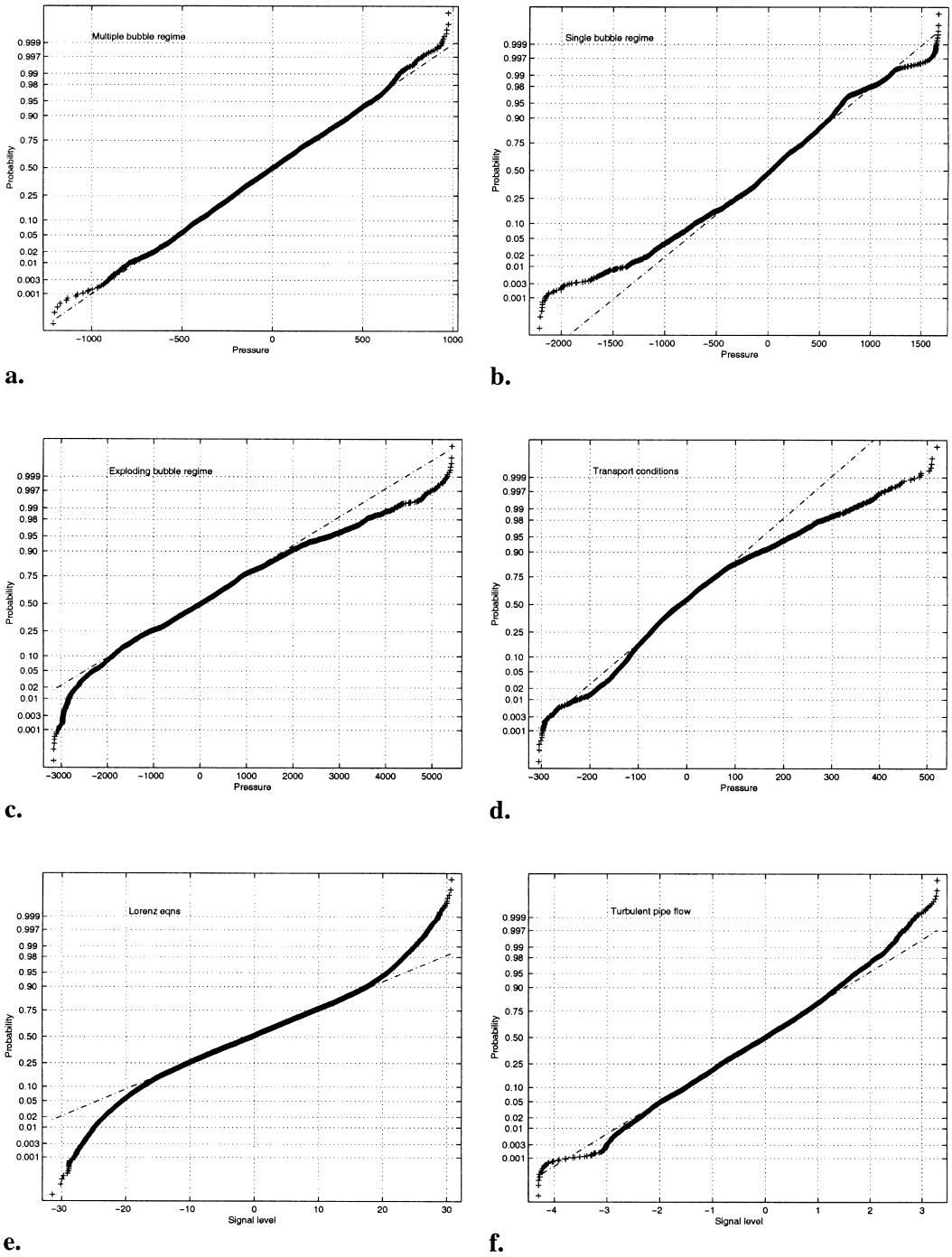

Fig. 8. Normal probability plots with dashed lines corresponding to normal distributions (based on 8000 samples): (a) multiple bubble regime, (b) the single bubble regime, (c) exploding bubble regime, (d) transport conditions, (e) the x-component of the Lorenz equations, and (f) velocity fluctuations of turbulent pipe-flow. The dashed curves correspond to a Gaussian distribution. Fluidized bed conditions according to Table 1.

a scale which is similar to the bubble frequency (cf. below), and there seems to be a correlation with respect to the bubble dynamics. The corresponding plots for the chaotic Lorenz system and for the turbulent pipe-flow are given in Fig. 9e and f, both characterized by a fast decay, reminding of the multiple bubble regime and transport conditions.

4.1.4. Frequency domain analysis

The differences in the dynamics of the four fluidization regimes are clearly seen in the frequency domain, Fig. 10a–d. These plots show the first 10 Hz (of 200 Hz measured) of the power spectra (Eqs. (9) and (10)) with linear scales on both axes, a representation which is suitable to illustrate dominant frequencies. The multiple bubble regime has a broad band of frequencies between 0 and 10 Hz with a maximum at about 2.5–3 Hz (Fig. 10a). The pressure fluctuations are influenced by a multitude of bubbles in the bed. In the single bubble regime, the dominant frequency of about 0.7 Hz of the bed pressure fluctuations represents the passage of the single bubbles (the second lower peak should be due to a period doubling). The strong periodicity appears as a narrow peak in the power spectrum. The difference in amplitude (that is in the energy of the signal) of the pressure fluctuations (cf. Fig. 7a and b) is seen on the scales of the vertical axes of the power spectra in Fig. 10a and b.

The exploding bubble regime is characterized by large voids, but the flow pattern is more complex than that of the single bubble regime (Fig. 7b and c), and the dominant frequency is not readily estimated from the time sequence. However, the power spectrum of Fig. 10c shows a pronounced peak (at about 1.3 Hz) with only a minor part of the energy in the range of 2–10 Hz. On one hand, the single and exploding bubble regimes appear different in time domain but similar in frequency domain. On the other hand, the time series of the exploding bubble regime (Fig. 7c) and in the transport conditions (Fig. 7d) look similar in frequency-content, but they have quite different power spectra (Fig. 10c and d). Under transport conditions no pronounced dominant frequency is measured, although the major energy is located below 4 Hz, Fig. 10d. Hence, a direct interpretation of the signal in time domain may lead to spurious conclusions.

The strong periodicity of the single bubble regime can be illustrated by simply counting the number of major peaks in the time series. The dominant frequency obtained in this way becomes, in the 0.6 m/s case in Fig. 7b, 7 peaks/10 s $\Rightarrow$ 0.7 Hz, and for another run at 1.1 m/s (not shown): 10 peaks/10 s $\Rightarrow$ 1 Hz. These values are very well in agreement with the power spectra (0.68 Hz, Fig. 10b, and 0.91 Hz, respectively), which are based on the entire pressure signal (1967 s). Together with the appearance of this almost perfect periodicity of the bubble motion in this regime, we also observe a certain width of the peak in power spectra. The relation between such a strong periodicity *on a macro-scale* and the finer flow structures and non-linear behavior will be discussed in Section 4.4.

As pointed out in Section 3.3, a difference between the dominant frequency of the spectrum, f_d, and the average cycle frequency, f_c, indicates deviations from a perfect periodicity of the macro-flow, since f_c is based on the signal crossing its average. In Table 2 such a difference is seen to be present in the multiple bubble regime, with its broad-banded power spectrum in the low-frequency region, and also in the single and exploding bubble regimes, both having sharp peaks in the power spectra. In fact, the ratio of f_c to f_d is similar for the three regimes ($2.1 < f_c/f_d < 2.7$), which indicates that the finer structures have a significance in all cases since

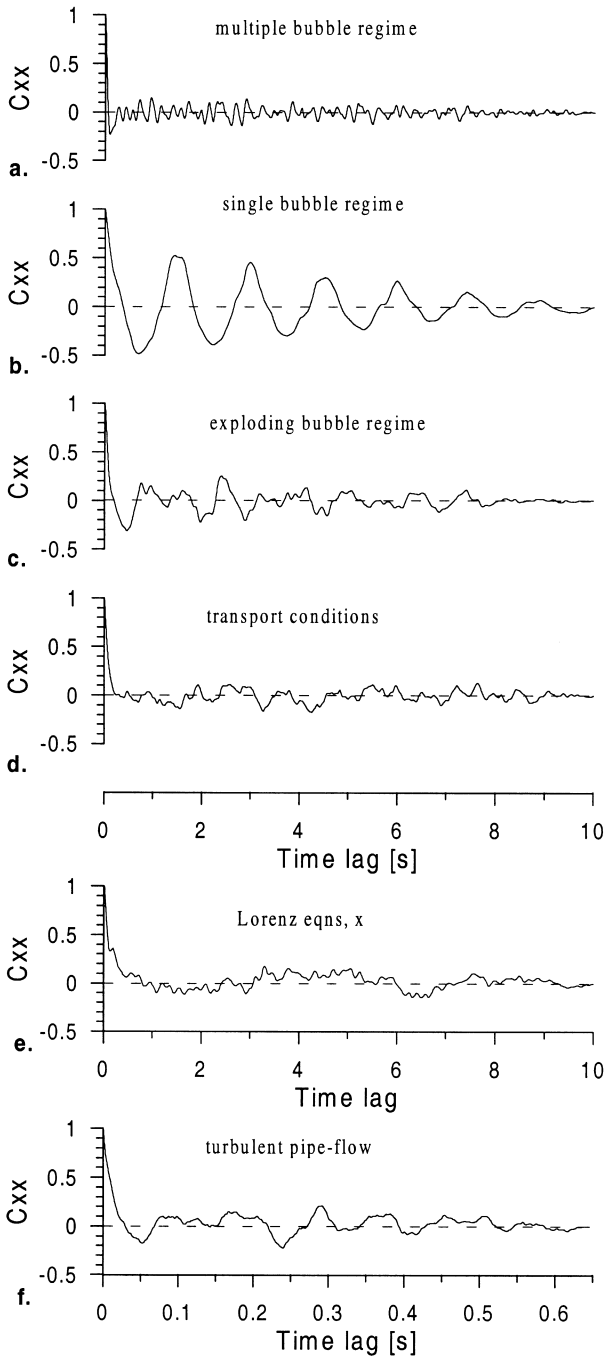

Fig. 9. Autocorrelation function based on 4000 samples (10 s): (a) multiple bubble regime, (b) single bubble regime, (c) exploding bubble regime, (d) transport conditions, (e) x-component of the Lorenz equations (arbitrary time scale), and (f) velocity fluctuations of the turbulent pipe-flow. Fluidized bed conditions according to Table 1.

f_c exceeds the region of the dominant frequency. Under transport conditions there is no meaning in defining a dominant frequency and f_d given in Table 2 is simply the frequency corresponding to the maximum amplitude in the power spectrum.

Finer structures in the frequency domain are shown in Figs. 11 and 12, presenting the power spectra over a range of frequencies up to the Nyquist frequency of 200 Hz in Figs. 11a and 12 and up to 20 Hz in Fig. 11b and c. To study the fall-off with frequency, the spectra are plotted on a logarithmic vertical axis vs. the logarithm of frequency or vs. frequency on a linear scale. A power-law fall-off, $P_{xx} \sim f^{-\alpha}$, gives a straight line in a logarithmic plot and an exponential fall-off, $P_{xx} \sim \exp(-f/\mu)$, gives a straight line in a semi-logarithmic plot.

In spite of the large difference between the multiple and single bubble regimes, judging from the visual low-frequency macro-structure of the flow, there is surprisingly little difference between the power spectra above about 2–4 Hz, or above frequencies of the order of the average cycle frequency, f_c. The range 2–4 Hz seems to be a transition range in the cases studied, and 4 Hz was selected as a starting point for the power-law and exponential fits. Above 4 Hz both spectra of Fig. 11 can be divided into two regions: a Region 2 between 4 Hz to about 10 Hz which can be fitted as either power-law (Fig. 11a and b) or exponential fall-off (Fig. 11c) with about equal accuracy, with α around 2 (or $1/\mu$ around 0.3); and a Region 3 from about 20 Hz up to the Nyquist frequency (200 Hz) with a steeper power-law fall-off (Fig. 11a), with α around 5, Table 2. The fall-off in Region 3 was determined from 20 Hz to 100 Hz, the latter value being below the resonance frequency of the pressure measurement set-up (>120 Hz, cf. Section 2). Fig. 12 shows basically the same pattern in the exploding bubble

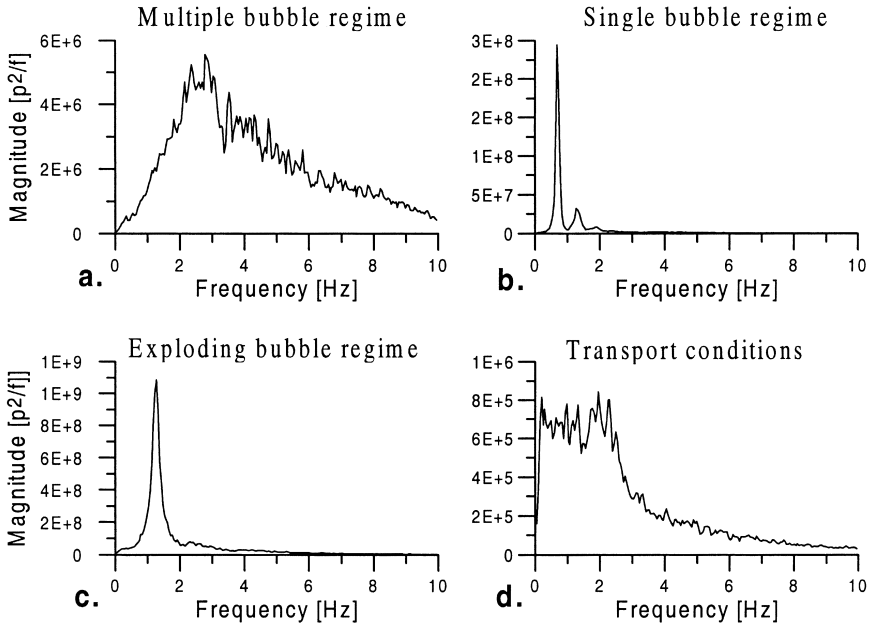

Fig. 10. Power spectra of: (a) multiple bubble regime, (b) single bubble regime, (c) exploding bubble rgime, and (d) transport conditions. The spectra, which are zoom-ins of the first 10 Hz, are averages of 96 sub-spectra, each cosisting of 8192 samples (corresponding to ≈ 20 s of measurement time). Operating conditions according to Table 1.

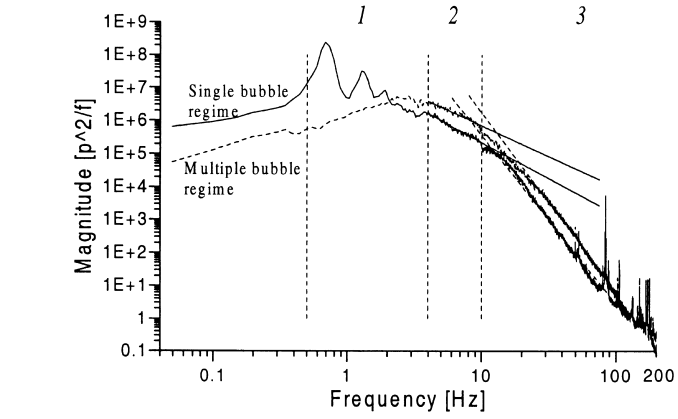

a.

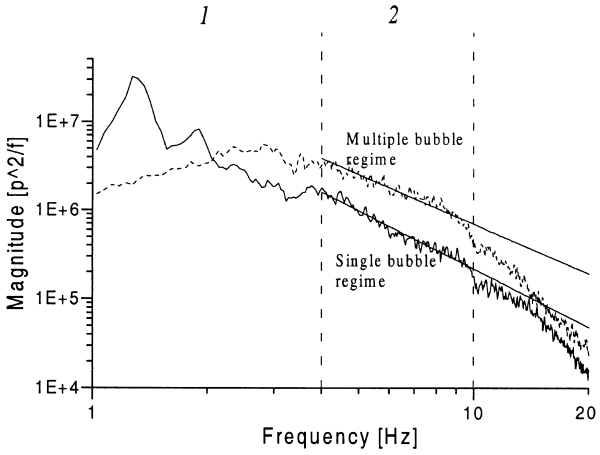

b.

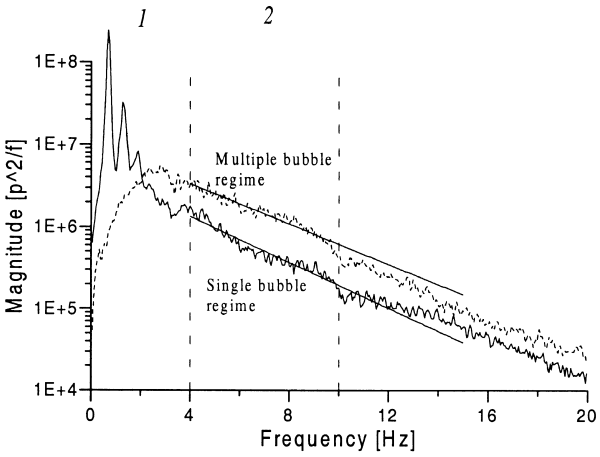

c.

Fig. 11. Power spectra of Fig. 10a and b (multiple and single bubble regimes) plotted on logarithmic (a, b) and semi-logarithmic scales (c). The solid lines are power-law (b) and exponential (c) fits in the range 4–10 Hz and the dashed lines (a) are a power-law fits from 20 to 100 Hz.

regime (Fig. 12a) and under transport condition (Fig. 12b); the spectra can be divided into three regions. The fall-off in Region 2 of the exploding bubble regime is somewhat steeper than for the other cases (Table 2), and Region 3 is less steep with $\alpha \approx 4$. As is clear from Figs. 11a, 12a and b, Region 3 cannot be fitted exponentially.

The possibility of fitting Region 2 both as power-law and exponentially may be partly due to the limited range of frequencies covered by this region which, however, contains a substantial amount of the energy of the signal. At this stage, it is premature to draw any conclusion about the system being (intermediately) chaotic based on the fits (cf. Nowak et al., 1993; Ding and Tam, 1994).

Fig. 12c and d present power spectra of the x-component of the chaotic Lorenz system (Eq. (1)) and of the measured velocity fluctuations, $\acute{u}(t)$, of the turbulent pipe-flow. As expected (Frisch and Morf, 1981; Greenside et al., 1982; Sigeti, 1995a, 1995b), the spectrum of the Lorenz equations falls exponentially over the whole frequency range (the spectrum exhibit a straight line in a semi-logarithmic plot) and a power-law fit is not adequate as indicated by the

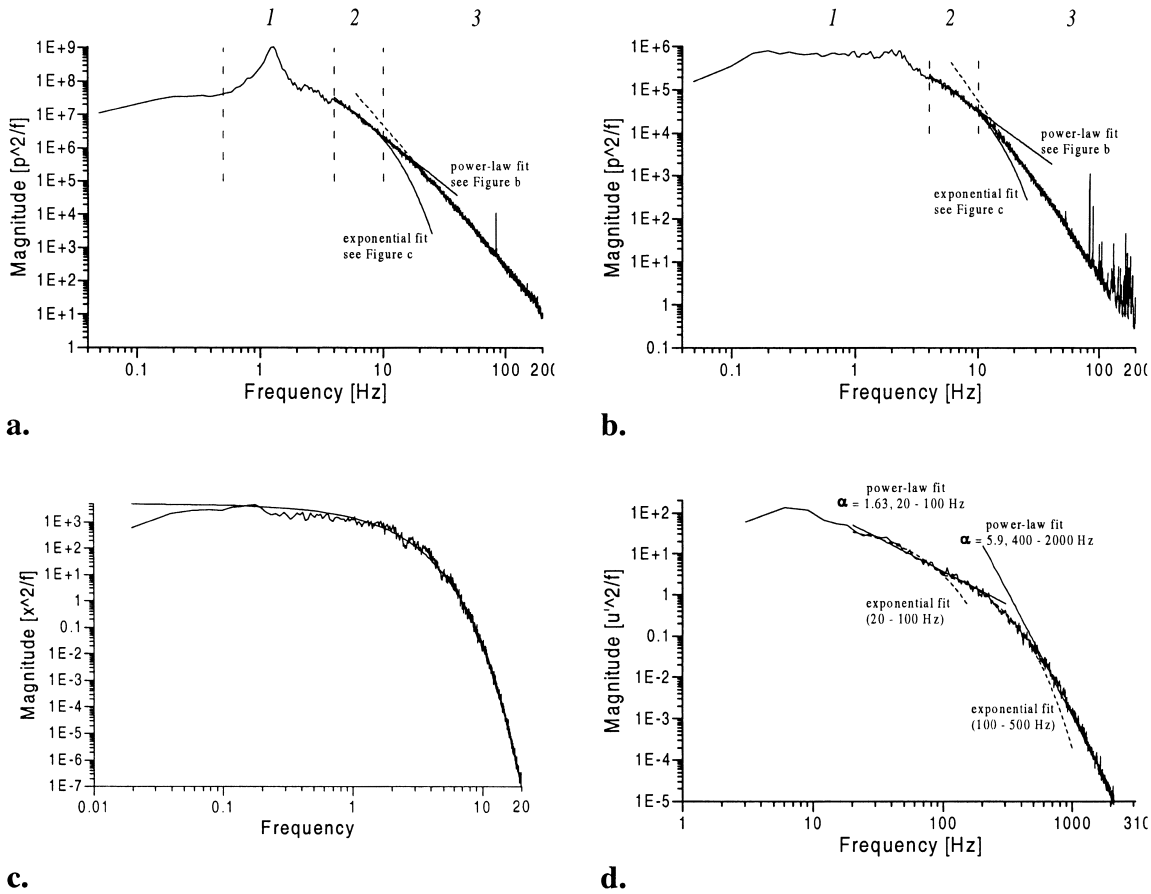

Fig. 12. The power spectrum plotted on logarithmic scales for: (a) the exploding bubble regime, (b) transport conditions, (c) the x-component of the Lorenz equations (Eq. (1) with the frequency scale arbitrarily chosen), and (d) velocity fluctuations of turbulent pipe-flow.

curvature obtained in Fig. 12c. From the power spectrum of the velocity fluctuations in the turbulent pipe-flow (Fig. 12d), we recognize the well-known Kolmogorov universal scaling law of the inertial sub-range (cf. Monin and Yaglom, 1975), corresponding to energy cascading, which on dimensional grounds can be shown to follow a power-law fall-off ($P_{xx} \sim f^{-\alpha}$) with $\alpha = 5/3 = 1.66$. There are numerous experiments confirming this fall-off for a vast range of Reynolds number in different applications (Saddoughi and Veeravalli, 1994). The corresponding fall-off in the spectrum of the pressure field of gas-flow turbulence, obtained on dimensional grounds (Monin and Yaglom, 1975; George et al., 1984 and references therein), is $\alpha = 7/3 \approx 2.33$, a value which has been confirmed experimentally from pressure spectra in turbulent free shear flows (George et al., 1984 and references therein) and in turbulent wall-layers (Schewe, 1983; Farabee and Casarella, 1991). At higher frequencies, in the dissipation region, the power spectrum of the velocity fluctuations of the turbulent pipe-flow falls steeper than with $\alpha = 5/3$ (cf. Monin and Yaglom, 1975). Exponential fits are not adequate, although the transition between the two regions can be fitted exponentially (Fig. 12d).

Sigeti (1995b) compares fall-off for different chaotic model systems, including the Lorenz model. Most of these model systems have, like the Lorenz model, a steeper fall-off than the fluidized bed data. However, chaotic model systems with a higher number of modes can also have a less steep, but still exponential, fall-off. The fourth-variable model given by Lorenz (1984), which, with the parameter studied by Sigeti, has one positive Lyapunov exponent, gives an exponential fall-off with $1/\mu = 0.326$, a value which is similar to the fluidized bed data of Table 2, especially when compared with $1/\mu = 0.323$ of the single bubble regime. In summary, it seems as if the fall-off in power spectrum of Region 2 is in-between what has been observed for chaotic model systems and the fall-off of the inertial sub-range of velocity spectra in turbulent flows. However, Region 2 covers a limited range of frequencies, and the comparison with literature data from model systems becomes difficult. The comparison has to be supported by comparisons made with other methods of time- series analysis. This is the case since the differences between the underlying mechanisms of the dynamics of the Lorenz model, the velocity fluctuations of the turbulent flow, and the pressure fluctuations of the fluidized bed, are unknown.

4.1.5. State-space analysis

Table 2 gives the results of the state-space analysis (D_{ML} and K_{ML}) and the non-linearity test (Z_{avg}) for the four flow conditions, the Lorenz model and the turbulent pipe-flow. The non-linearity test shows that the single bubble regime is non-linear with a value of Z_{avg}, which is similar to that of the Lorenz model. The other cases have values of Z_{avg} exceeding -3, and cannot be distinguished from a linear stochastic system. This does not mean that they necessarily are linear stochastic, but the outcome of the state-space analysis cannot be directly related to the presence of chaos. The general observation that non-linear (chaotic) systems have broad-banded power spectra (e.g., Moon, 1992; Abarbanel et al., 1993) seems not to be applicable to the present type of fluidized bed data. This is because the frequency range measured covers both macro-fluctuations and finer structures, and the latter are not revealed on a linear representation such as given in Fig. 10. Although the character of the fall-off at higher frequencies (Region 2) is similar to what has been observed for various non-linear and

chaotic systems, at the present stage of knowledge the fall-off cannot be used to quantify the system as being non-linear.

The maximum likelihood estimations of the correlation dimension, D_{ML}, for the fluidized bed data are in-between the values of the Lorenz model ($D_{ML} = 2.08$) and the turbulent pipe-flow ($D_{ML} = 8.01$), ranging from 2.55–6.23. This is in line with the results of the fall-off in power spectrum: the fluidized bed data have a fall-off between the chaotic model and the turbulent pipe-flow, Table 2. The value of D_{ML} of the single bubble regime ($D_{ML} = 2.55$) is of the same order as that of the Lorenz model ($D_{ML} = 2.08$). Note also the similarity in the result of the non-linearity test (Z_{avg}).

The dimensions of the fluidized bed data of this work are similar to those presented in literature, which are about 2 for low velocity slugging conditions, around 4 for bubbling conditions and up to 6 for higher velocities under turbulent or turbulent like conditions (van den Bleek and Schouten, 1993; Vander Stappen et al., 1993; Hay et al., 1995; Vander Stappen, 1996). Thus, low velocities with well-defined voids passing the bed, such as the single bubble regime of this work and the slugging regime (Vander Stappen, 1996), yield low dimensions (D_{ML} values of about 2 to 3) while the more complex macro-structure of the multiple bubble, transport and turbulent regimes results in higher dimensions, up to about 6. The conclusion is: the less complex the macro-flow, the lower the dimension. All values reported are between those of the chaotic Lorenz model and those of the turbulent pipe-flow.

Table 2 contains Kolmogorov entropy, K_{ML}, expressed in bits/cycle as well as in bits/s. The difference in entropy per cycle, K_{ML} (bits/cycle), is rather small and cannot directly be related to the complexity of the flow, like the dimension. This could be expected, since with complexity of the flow we mean the macro-structure. The average cycle frequency depends on the macro-structure of the flow. The more complex the flow, the higher the average cycle frequency and the shorter the average cycle time. The power spectra (Figs. 11 and 12) and Table 2 show that the fine structures of the flow (Regions 2 and 3 in the power spectra) occur for time scales shorter than the average cycle time (at $f > 4$ Hz). When expressed in bits/s the Kolmogorov entropy is directly linked to the time scale of the system, and the time scale of the macro-structure (Region 1 of spectra) will influence the result. Thus, just as in the case of the dimension: the more complex the flow, the higher K_{ML} when expressed in bits/s. Note that, in spite of $Z_{avg} > -3$ in the more complex cases, these may also be non-linear, although this cannot be shown.

The Kolmogorov entropy shows a tendency to be lower in cases with less complex macro-flow. In the slugging regime, Vander Stappen et al. (1993) and Vander Stappen (1996) reported K_{ML} of around 4 bits/cycle, whereas for bubbling conditions the values are around 5 (van den Bleek and Schouten, 1993; Vander Stappen et al., 1993; Vander Stappen, 1996). The transition from a fixed bed to a bubbling regime with an increase in fluidization velocity was reflected in a corresponding transition in the values of K_{ML} (bits/cycle). When expressed in bits/s, K_{ML} shows a clear dependence on the macro-structure of the flow and in this form it has been utilized to explore fluidization regimes (e.g., Vander Stappen et al., 1993; Zijerveld et al., 1997a; 1998). The Kolmogorov entropy expressed in bits/second incorporates both the information lost during an average time-cycle and the information loss in real time. Thus, if the entropy in bits/cycle remains constant, a change in entropy when expressed in bits/s may

not, as mentioned in Section 3.3, correspond to a fundamental change in the character of the time series. Section 4.3 will discuss this in more detail.

4.2. Intermittent structures

Chaotic systems have a strongly intermittent structure, which, in time domain, is only revealed by high-pass filtering of the time series representing the system (e.g., Greenside et al., 1982). Fig. 13 exemplifies high-pass filtered time series of the pressure fluctuations. Again, the time series of the Lorenz system and of the velocity fluctuations in the turbulent pipe flow are included for comparison. Intermittent time series have quiescent periods with occasional bursts in the amplitude. In this sense, there is a strong similarity between the Lorenz equations and the single bubble regime with a pronounced intermittency in both cases (Fig. 13a and b) whereas the time series from the transport conditions resembles the turbulent pipe flow, both with a similar intermittent structure (Fig. 13c and d) which is not as clear-cut as those of the Lorenz model and the single bubble regime.

Flatness, F (Eq. (6)), can be used as a measure of intermittency. Fig. 14a and b give F for the six time series treated, high-pass filtered with different filter-frequencies. A base level of 3, which corresponds to Gaussian white noise, is indicated in the figures by a horizontal dashed line. The F-values of the signals listed in Table 2 correspond to 'zero' filter frequency (no filtering, other than that during measurements for removing the average of the signals) in Fig. 14. Fig. 14a shows flatness vs. filter-frequency for the turbulent pipe-flow data and for the Lorenz model. As expected (see Kuo and Corrsin, 1971; Frisch and Morf, 1981), the flatness of the velocity fluctuations of the turbulent pipe-flow increases throughout the inertial sub-range up into the dissipation range and then decreases due to the influence of measurement noise. The flatness of the chaotic Lorenz system (Fig. 14a) shows a continuous increase with filter frequency and, eventually, at high filter frequencies F becomes very large, values up to 1000 were calculated. Similar results were reported by Greenside et al. (1982). It is important to note that high-pass filtering of a stochastic model system (viz., the Langevin equation) with a power law spectrum ($\alpha = 4$) was shown by Greenside et al. to approach a flatness of 3 with increased filter frequency.

Fig. 14b shows that high-pass filtering of the fluidized bed data strongly increases the flatness with increased filter frequency, indicating a strong intermittency. In the multiple bubble regime, the increase in F with filter frequency is less steep and passes a maximum (the entire decrease is not shown in Fig. 14b), a result which resembles that of the turbulent velocity fluctuations of the pipe-flow (Fig. 14a). The single bubble regime gives large values of F (up to 1000) as the filter frequency is increased, similar to the chaotic Lorenz system. The flatness of the time series of the exploding bubble regime also approaches large values with an increase in filter frequency, but not as large as in the single bubble regime. Except for the multiple bubble regime, there is a strong intermittency already in Region 2 of the power spectrum.

The time-series analysis methods employed, roughly put the four significantly different fluidization modes in-between the chaotic Lorenz system and the turbulent pipe flow. In spite of the periodic-like behavior on a macro-scale of two of the time series (the single and exploding bubble regimes), the pronounced intermittent structure shown to occur at

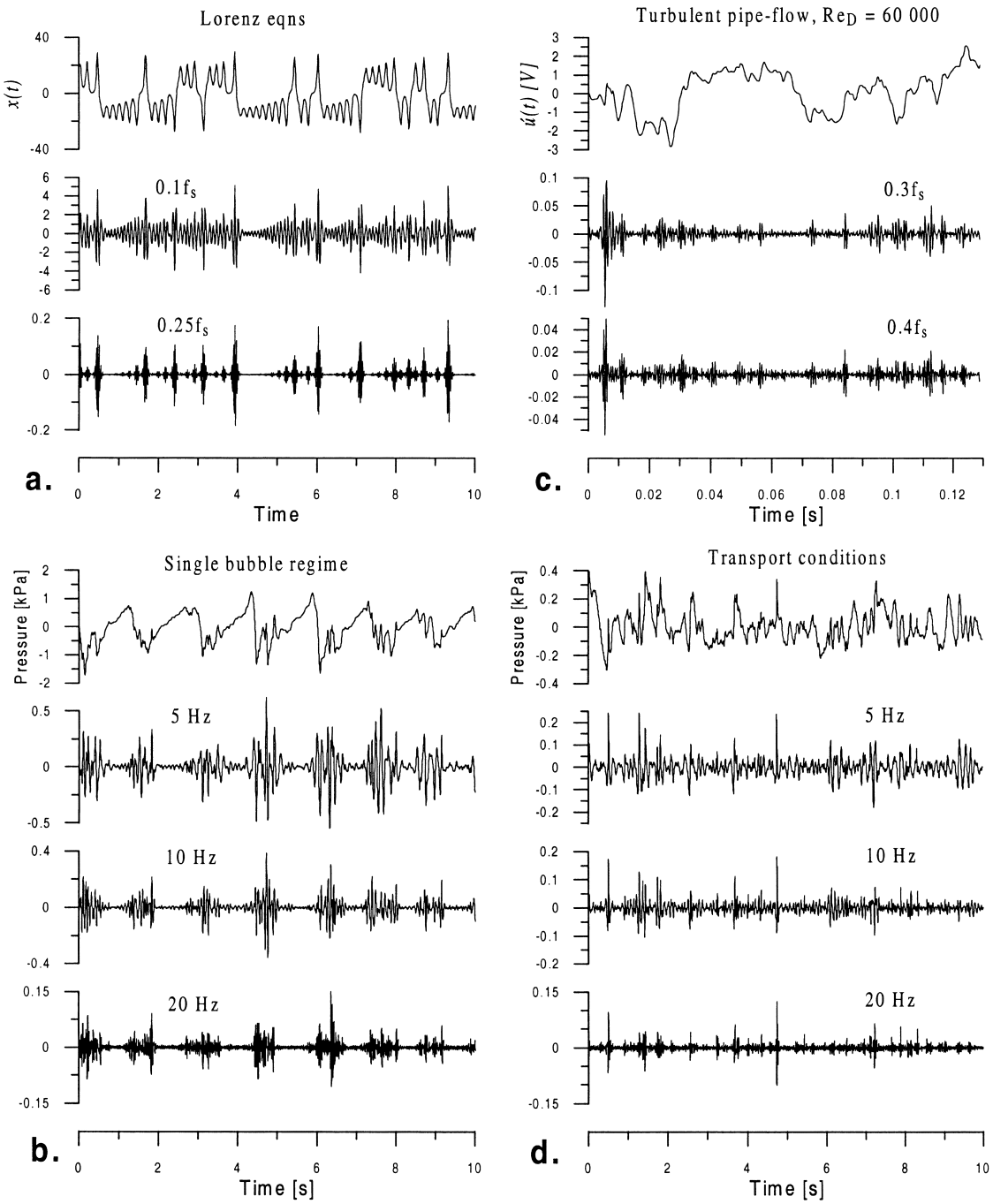

Fig. 13. Examples of high-pass filtered time sequences. The time scale of Figure a is arbitrarily chosen (1000 points/10 s).

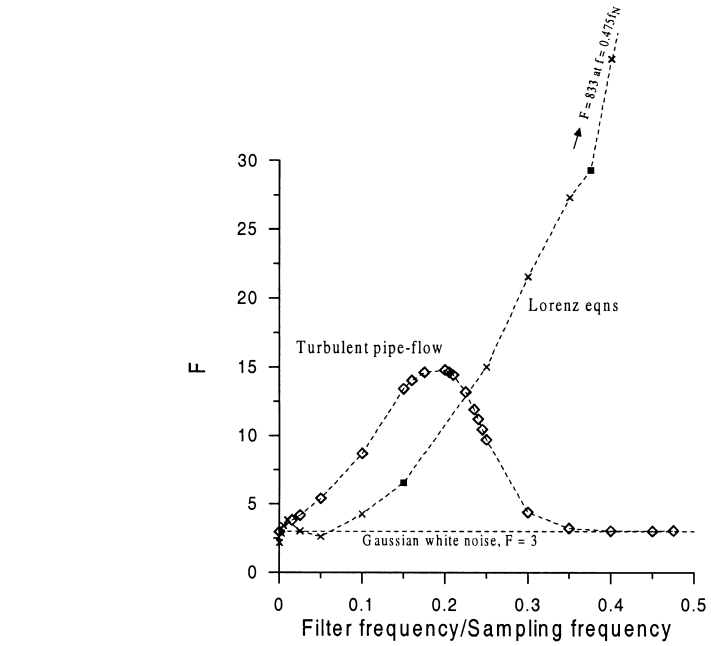

Fig. 14. Flatness, F vs. high-pass filter frequency for: (a) the x-component of the Lorenz equations and the turbulent velocity fluctuations, and (b) the four fluidiization regimes studied. Fluidized bed conditions according to Table 1.

higher frequencies indicates that non-linearities and chaos may be present in these cases. The intermittency at higher frequencies corresponding to Region 2 is similar to what was observed in the fall-off region of turbulent velocity and pressure spectra.

The present results give us no direct information on the physics behind the measured pressure fluctuations at higher frequencies (Regions 2 and 3). However, there is an analogy between features observed in the pressure spectra of the two-phase flow and from those of turbulent one-phase flow. Thus, some factors make it tempting to speculate on the presence of large scale fluctuations with characteristics similar to the dynamics of gas-flow turbulence, i.e., energy cascading starting at time and length-scales corresponding to the frequency and size of the bubbles:

1. The presence of intermittency at high frequencies.
2. The high Reynolds numbers of the gas flow. This (*Re* at least 100, Tennekes and Lumley, 1972) is a prerequisite for local isotropy (similarity at small scales), which results in the above-mentioned power-law fall-off in velocity and pressure spectra. The characteristic length-scale of the flow in the fluidized bed is not known with certainty. Under the assumption that the gas flow within and through the bubbles (or between the strands in case of no bottom bed) is the major contribution to the large scale velocity fluctuations in the gas flow, thus assumed to generate large scale vortices, a Reynolds number based on the bubble diameter can be defined, $Re_{D_b} = uD_b\rho/\mu$ (where ρ and μ represent density and viscosity of the gas). This Re_{D_b} ranges from 4000 to 60,000 in the four cases given in Table 1, and satisfies the criterion given by Tennekes and Lumley. The gas velocity through the bubble/between strands is taken as the superficial gas velocity, u. It is likely that this velocity is underestimated and, thus, the estimations of the Re_{D_b}-values are conservative.
3. Previous studies have shown pronounced fluctuations in gas velocity above the surface of fluidized beds (Pemberton and Davidson, 1984 and references therein). By using hot wire anemometry, Pemberton and Davidson measured turbulent velocity fluctuations of the same order as the mean fluidizing velocity. The irregularity of the fluctuations in gas-flow was due to the eruption of the bubbles at the bed surface, forming flow structures which the authors named 'ghost bubbles'.
4. Tamarin and Livshits (1977) and Livshits and Tamarin (1980) performed direct measurements of solids and gas velocity fluctuations in a fluidized bed and the spectra of these measurements show a fall-off which is similar to turbulent one-phase flow, with the fall-off independent of the macro structure of the flow. They explained this with a gradual transfer of energy from large to small vortices which eventually dissipates at scales comparable with the particle diameter. It should be pointed out that the turbulent energy cascading in single phase flow for Reynolds numbers and characteristic lengths similar to those given above, occurs at much smaller scales (higher frequencies) and so does turbulence due to interaction of gas and particles in dilute flow (e.g., Stock, 1995).

The question, which remains to be answered, is if the physics behind the large scale fluctuations of Regions 2 and 3 is similar to turbulence as suggested by Tamarin and Livshits. Further measurements are required to answer this question.

The transitions between the regimes are continuous, and it is of interest to see the outcome of the time-series analysis from a continuous change in the operating conditions. This is

performed in the next section, where the CFB-unit is operated over a wide range of fluidization velocities, covering the single and exploding bubble regimes and transport conditions.

4.3. Single bubble regime to transport conditions

Fig. 15 summarizes the results of the time-series analysis over the entire range of gas velocities studied. Evaluation of video recordings confirms the amplitude of the fluctuations, Fig. 15a, to be strongly dependent on the size of the bubbles. In the single bubble regime, the amplitude (standard deviation) goes through a maximum when a major part of the bed is lifted by the bubble to a location above the 0.2 m pressure tap. Fig. 16 shows that within the single and exploding bubble regimes, there is an increase in the average voidage, ε, of the bottom bed together with a decrease in bottom bed height, H_x. In the exploding bubble regime, the effect of bubbles lifting the bed is less significant or, at high velocities, not observed at all. Since the maximum bubble size is limited by the bed height, the small reduction in bed height leads to somewhat smaller exploding bubbles and to lower amplitudes. The decrease in average solids concentration with an increase in velocity should contribute to the smaller amplitude. On the other hand, the velocity of the gas passing through the bubbles increases substantially, and this makes the flow pattern more complex than at lower velocities, and a splash zone forms above the bed. The moderate increase in voidage in the bed during an increase of gas velocity means that almost the entire excess gas flow passes the bed as through-flow through the exploding bubbles (Johnsson et al., 1991; Zijerveld et al., 1997b). It is not possible to attribute the decrease in amplitude of the fluctuations to either the decrease in solids concentration and bed height or to a change in the dynamics. Under transport conditions the amplitude is low.

Skewness, S, and flatness, F, are not included in Fig. 15, since they are similar to those of a Gaussian distribution when calculated from the unfiltered signals (Table 2). Hence, S and F provide no useful information on the flow regimes.

Fig. 15b compares the dominant frequency of the power spectrum, f_d, and the average cycle frequency, f_c. Under transport conditions (cf. Fig. 10d), a clear dominant frequency is lacking and the frequency corresponding to the maximum amplitude in the power spectrum is given instead of f_d (filled symbols in Fig. 15b). All cases show a significant difference between f_d and f_c, indicating a deviation from periodicity, and f_d and f_c depend differently on gas velocity. Whereas f_d remains almost independent of velocity, f_c increases with velocity, indicating an increased complexity of the flow which leads to a shortened time-scale. Under transport conditions the maximum amplitude of the spectra yields no valuable information, since the location of the 'dominant' frequency in the wide Region 1 is not well-defined (Fig. 10d).

The change in fall-off of Region 2 in power spectrum with velocity is given in Fig. 15c. The fall-off is not constant but changes continuously with velocity in the three regimes shown. The fall-off under transport conditions is similar to that of the pressure field of gas-flow turbulence ($\alpha = 7/3 \approx 2.33$). When the flow is dilute, we can expect the gas-particle dynamics to be nearer turbulent gas-phase flow than under the denser conditions studied which, perhaps, explains the fall-off to be near the 7/3 fall-off of single phase flow. At low velocities, in the single bubble regime, the two phases are sharply separated in space-domain and Region 1 of the spectrum is directly linked to the macro-structure of the flow. Therefore, we may assume the fall-off in Regions 2 and 3 to correspond to gas-phase fluctuations, which are more or less influenced by

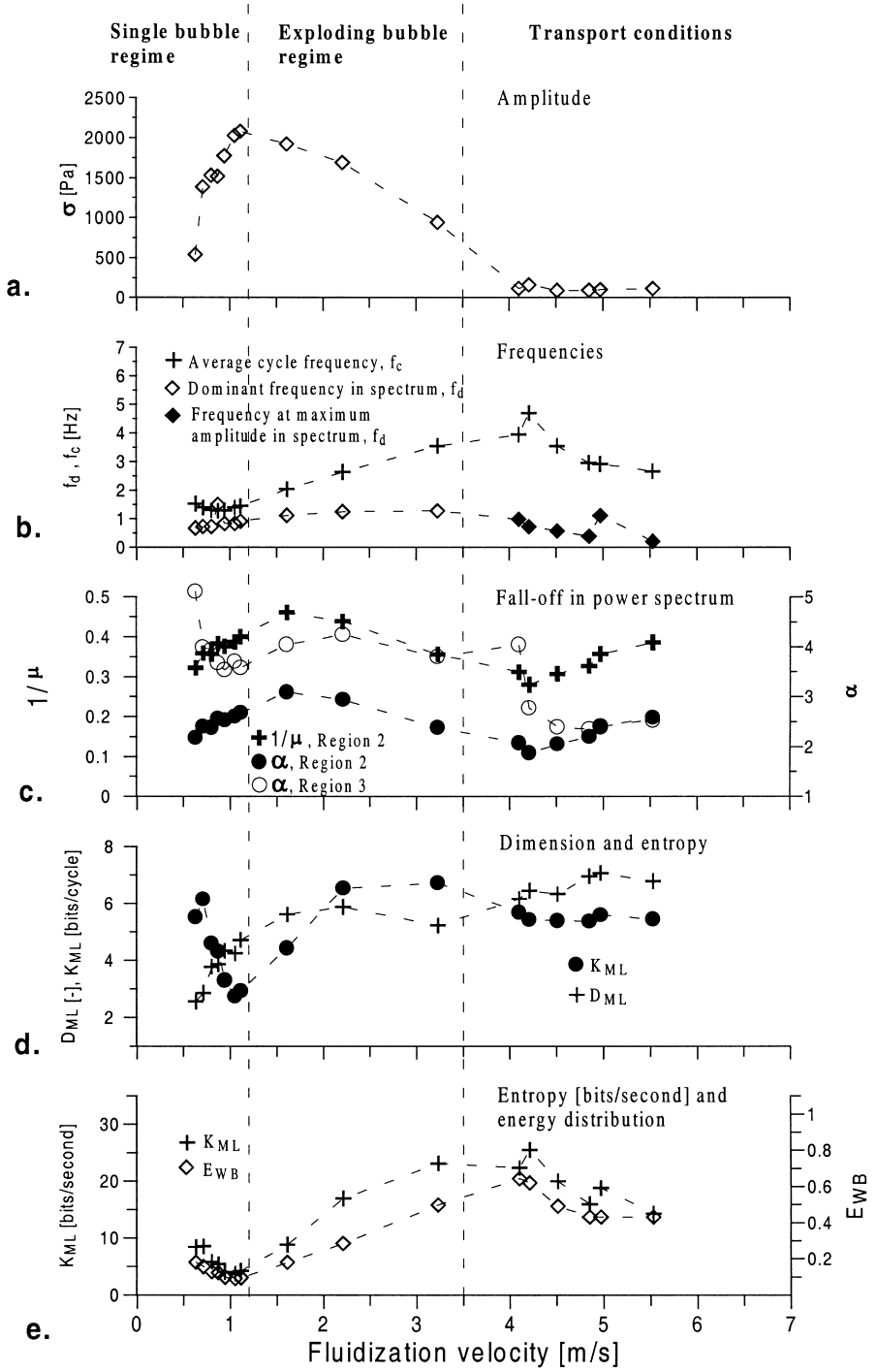

Fig. 15. Summary of the results of the time-series analysis applied on the time series of pressure fluctuations for the different velocities investigated in the CFB-unit: (a) standard deviation (σ), (b) dominant or maximum frequency in power spectrum (f_d) and average cycle frequency (f_c), (c) fall-off in power spectra (cf. Figs. 11 and 12), (d) correlation dimension (D_{ML}) and Kolmogorov entropy (K_{ML}) in bits/cycle, and (e) Kolmogorov entropy in bits/s and wideband energy (E_{WB}).

the presence of particles. At intermediate velocities the fall-off passes a maximum as the velocity is increased. This may be interpreted as the existence of a strong interaction between the two phases at time scales corresponding to Region 2 in the power spectrum. The interaction gets stronger at higher velocities, but for more dilute suspensions the influence of the dense phase on the measured pressure fluctuations becomes smaller and this could result in a maximum in fall-off.

Region 3 gives a power-law decay in all cases studied. The decay constant, α, of Region 3 is incorporated in Fig. 15c. Except for the lowest and highest velocities, the fall-off in Region 3 is fairly constant with a power-law decay of around 4. At the lowest velocities, the energy in Region 3 is very low and an interaction with the measurement-tube may exist. Considering estimates of the particle relaxation time (Peirano et al., 1998), it may be assumed that the time scales of Region 3 ($f > 20$ Hz $\Rightarrow$ t $<$ 50 ms) correspond to gas-flow fluctuations. A similar fall-off ($\alpha = 5$) was observed by Löfdahl et al. (1996) in spectra of pressure fluctuations of gas-flow turbulence in a turbulent wall-layer measured by a small silicon pressure transducer, however, at considerably smaller time scales.

The maximum likelihood estimation of the correlation dimension, D_{ML}, is a measure of the complexity of the attractor in state-space. D_{ML} is given in Fig. 15d: the higher the velocity, the more complex is the attractor with D_{ML} ranging from 2.55 to 7. The low-velocity cases of the single bubble regime yield D_{ML}-values below 5. In this regime, there is a continuous increase in D_{ML} with an increase in velocity indicating an increased complexity of the flow. Within the exploding bubble regime the dimension remains fairly constant ($D_{ML} \approx 5.5$) with an increase in velocity. Under transport conditions D_{ML} changes from about 6 to 7 in the velocity range studied.

Calculated values of D_{ML} should be compared with the results of a non-linearity test, since stochastic systems with power-law spectra have also shown to produce finite values of the correlation dimension. We have already shown that the measured time series exhibits a strong intermittency with an increase in flatness, F, at high frequencies, indicating a non-stochastic behavior. In Section 4.1, the data from the single bubble regime were shown to be non-linear (Table 2), whereas the data from the other regimes could not be distinguished from a linear

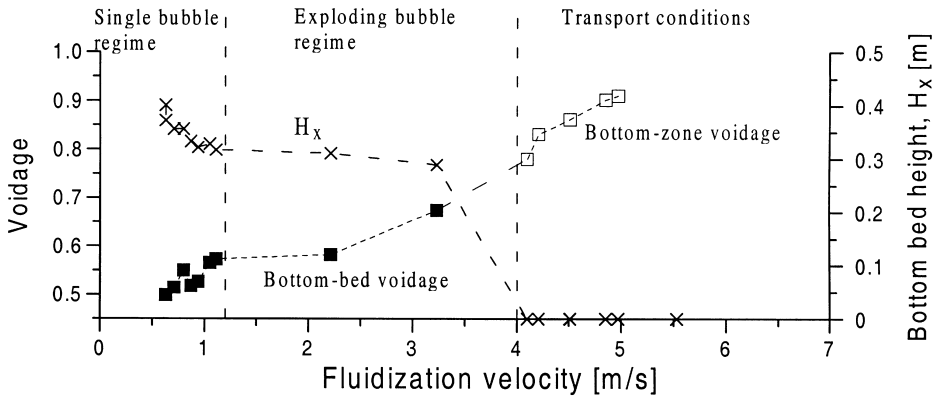

Fig. 16. Bottom bed voidage, ε, and bottom bed height, H_x, at different velocities.

stochastic system. Fig. 17 summarizes the calculated values of the correlation dimension, D_{ML}, and the outcomes of the non-linearity test (Z_{avg}) for all cases studied. Z_{avg} is not a measure of non-linearity but expresses the statistical level of significance at which the hypothesis of non-linearity can be approved or rejected. The strong correlation between D_{ML} and Z_{avg} in Fig. 17 may be expected. Systems with a high dimension, having many modes, are difficult to distinguish from stochastic systems, having an infinite number of modes. In agreement with the previous section, all fluidized bed data are in-between the Lorenz model and the turbulent pipe-flow measurements, and the correlation dimension is related to the macro-structure of the flow; the more complex the flow-picture is, the higher the dimension becomes. Thus, the multiple bubble regime and the velocities corresponding to transport conditions have high dimensions and $Z_{avg} > -3$ and non-linearity cannot be claimed. However, as shown in the previous section, flatness grows with filter-frequency for all time series. This would not be the case if the data were completely stochastic (having power-law spectra). Fig. 17 shows that when the correlation dimension exceeds 5.5, non-linearity cannot be claimed for the data investigated.

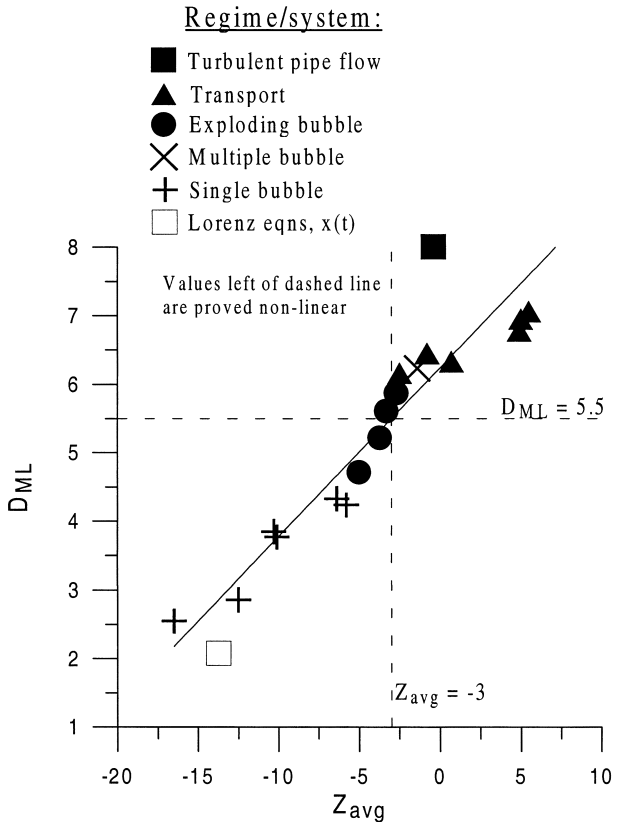

Fig. 17. Correlation dimension (D_{ML}) plotted in relation to the outcome of the non-linearity test (Z_{avg}), Z_{avg} express the satistical level of significance at which the hypothesis of non-linearity can be approved or rejected. It is not a measure of non-linearity.

The Kolmogorov entropy, K_{ML} (bits/cycle), in Fig. 15d differs from Section 4.1, where the entropy was fairly similar for the four regimes. Indeed, K_{ML} is similar for the exploding bubble regime and under transport conditions, but an increase in gas velocity in the single bubble regime results in a significant decrease in K_{ML} down to a minimum of $K_{ML} = 2.3$ bits/cycle. The visual (video) observations confirmed that an increase in velocity in this regime results in larger bubbles which, at the velocity of the lowest K_{ML} value, almost fill out the entire cross-section of the bed, and the bubbles are clear-cut and symmetric. Furthermore, with an increase in velocity the average cycle frequency becomes lower (Fig. 15b) and the power spectrum more narrow (Fig. 15e). A further increase in velocity breaks up the single bubble structure and the more complex exploding bubble regime is entered. Fig. 15e incorporates K_{ML} expressed in bits/s showing a similar dependence on velocity as obtained in Fig. 15d, but with differences such as a lower decrease with velocity in the single bubble regime.

The observations made in this section give rise to several questions. Are there any general differences between the non-linear time series and those which cannot be proved to be non-linear, i.e., between those for which $D_{ML} < 5.5$ and those for which $D_{ML} > 5.5$ according to Fig. 17? Can the state-space analysis be divided between macro-structures and finer structures of the flow? Or, more specifically, is it possible to link the difference between the regions in the power spectrum to the non-linear analysis? Is it possible to use f_c as demarcation between the macro-structure and the finer structures in the frequency domain (between Regions 1 and 2 in power spectrum)? The next section addresses these questions.

4.4. Comparison of frequency domain and state-space analysis

The dominant frequency (if present) in a power spectrum of the pressure fluctuations, yields information related to the bubble motion (see Sun et al., 1994 and references therein). Because of the complexity of the flow, and having the intermittency at frequencies above the dominant frequency in mind, it is more interesting to look at the *distribution of frequencies* in the power spectrum than to go beyond only the dominant frequency and to compare the amount of energy in Regions 1–3 of the power spectrum with the values of K_{ML}, D_{ML} and f_c. Except for the single bubble regime, an increase in gas velocity results in a wider power spectrum with energy transferred from Region 1, mainly to Region 2 but also to Region 3. In the single bubble regime, we noted a decrease in K_{ML} together with a narrowing of the power spectrum (not shown in plots) with an increase in gas velocity.

Utilizing Parsevals theorem (Eq. (13)), the change in energy outside Region 1 as a consequence of a change in operational condition/regime can be determined. The frequencies limiting Region 1 can be chosen as 0.5 and 2 Hz, i.e., only the macro-structure of the flow induced by the bubble motion is included in Region 1. For spectra with a clear peak, only a small amount of energies are found at frequencies below 0.5 Hz. Spectra measured under transport conditions have a more or less continuous decline in energy in Region 1 (Fig. 12b), and in this case the limit was extended to the lowest frequency in the spectrum, Δf. The energy in Regions 2 and 3 can be expressed in relation to the total energy of the power spectrum and is called the wide band energy, E_{WB},

$$E_{\mathrm{WB}} = \frac{\left[\sum_{f=\Delta f}^{0.5\ \mathrm{Hz}} P_{xx}(f) + \sum_{f=2\ \mathrm{Hz}}^{f_N} P_{xx}(f)\right]}{\sum_{f=\Delta f}^{f_N} P_{xx}(f)}. \tag{23}$$

Applying 4 Hz instead of 2 Hz as demarcation between Regions 1 and 2 did not significantly affect the result. E_{WB} is included in Fig. 15e, where a strong correlation is seen between E_{WB} and K_{ML} expressed in bits/s, also illustrated in Fig. 18. There is a substantial increase in E_{WB} with increased velocity in the exploding bubble regime and a decrease in E_{WB}, as a consequence of the narrowing of the power spectrum, in the single bubble regime and under transport conditions. From the increase in E_{WB} and K_{ML} with velocity in the exploding bubble regime, it can be concluded that, in spite of the major frequency remaining almost constant, there is a substantial increase in the finer structures of the flow. Fig. 18 also includes the multiple bubble regime which has a wide spectrum due to the many bubbles present in the bed.

The major contribution to the change in E_{WB} is from frequency ranges which have a strong intermittent structure. Since intermittency is a characteristic of non-linear systems, as discussed by Frisch and Morf (1981), Manneville (1981), Greenside et al. (1982) and Provenzale et al. (1993), a relation between the amount of energy in the intermittent frequency range and the degree of predictability of the time series (as quantified by the Kolmogorov entropy) is expected (Fig. 18).

Before we investigate the relation between E_{WB} and K_{ML} in bits/cycle and between E_{WB} and D_{ML}, we recall the differences between the values of K_{ML} in bits/cycle and K_{ML} in bits/s (Fig. 15d,e and Table 2). Such a difference is expected. The loss of information during an average

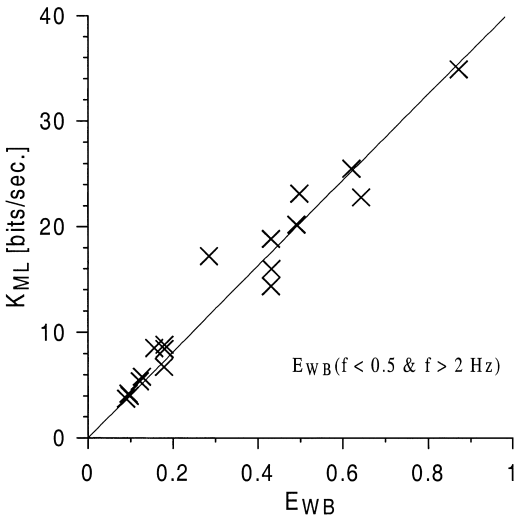

Fig. 18. Kolmogorov entropy (K_{ML}) in bits/s vs. the wide band energy (E_{WB}).

cycle ($1/f_c$), K_{ML} (bits/cycle), is not likely to vary in the same manner as the loss of information related to the absolute time scale, K_{ML} (bits/s), since there are strong differences between the average cycle frequencies, f_c, of the regimes (Fig. 15b). Frequencies above f_c are within Region 2, and f_c could be seen as a frequency dividing the macro-structure from the finer structures of the time series in state-space.

Fig. 19 relates K_{ML} in bits/s to the average cycle frequency. The figure shows that when $D_{ML} > 5.5$, i.e., in cases which could not be distinguished from linear stochastic systems, K_{ML}, if expressed in bits/cycle, varies little with cycle frequency; a least square fit to the data for $D_{ML} > 5.5$ gives $K_{ML} = 5.61$ bits/cycle. On the other hand, the data which were proven to be non-linear show strong variations in K_{ML} per cycle, as also seen in the single bubble regime in Fig. 15d. This result supports the following interpretation of the relation between Kolmogorov entropy in bits/cycle and the wide band energy, E_{WB}, shown in Fig. 20, which is different from the corresponding relation for K_{ML} expressed in bits/s of Fig. 18. Thus, when $D_{ML} < 5.5$ there is an increase in entropy, both per average cycle and per time unit as the energy is transferred from the macro-structure of Region 1 to the fine structures of Regions 2 and 3. When

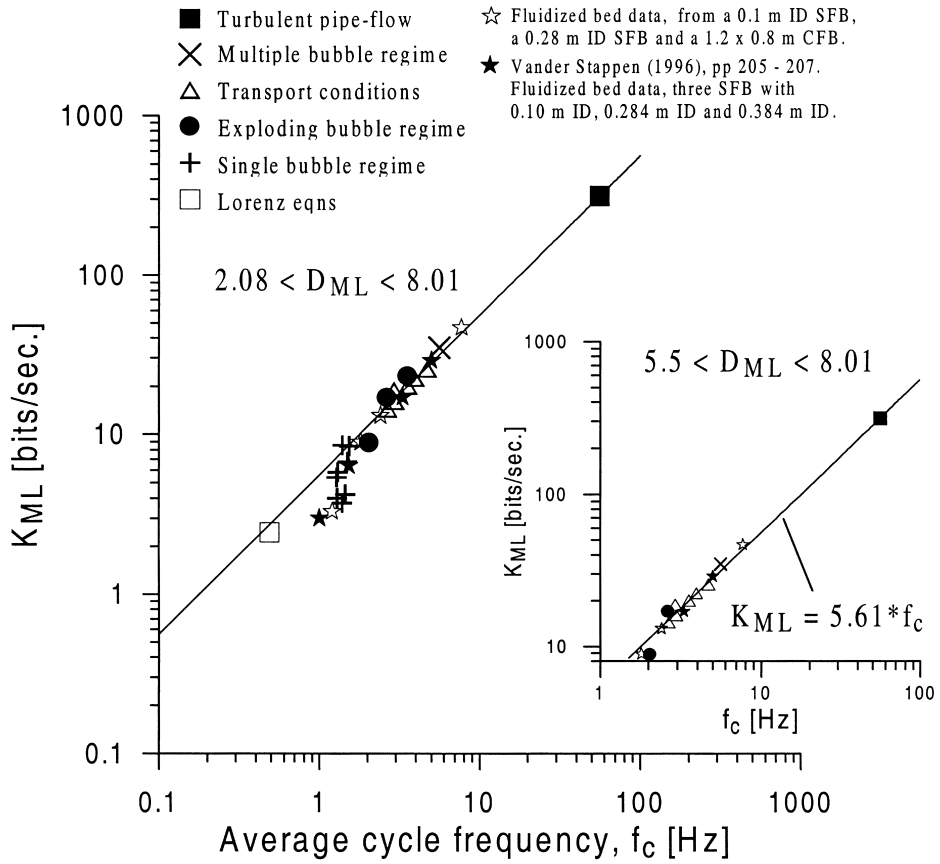

Fig. 19. Kolmogorov entropy (K_{ML}) in bits/s vs. average cycle frequency (f_c). The frequency scale is arbitrarily chosen (same as in Fig. 16a) for the Lorenz equations.

$D_{ML} > 5.5$, which occurs when E_{WB} exceeds 20% of the energy of the time series (Fig. 20), an increase in the amount of energy in the finer structures, E_{WB}, does not influence K_{ML} per cycle, whereas there is a proportional increase in K_{ML} when related to the time unit. For $D_{ML} > 5.5$, the increase in K_{ML} (bits/s) with an increase in E_{WB} is then entirely due to an increase in the average cycle frequency, which, as can be seen from Fig. 15b, occurs within Region 2 of the power spectrum (with 2 Hz as demarcation between Regions 1 and 2 as in Eq. (23)). For $D_{ML} < 5.5$, on the other hand, the increase in K_{ML} per second with an increase in E_{WB} is both due to an increased complexity of the macro-structure of the flow (increase in f_c when f_c is within Region 1, Fig. 15b) and due to an increase in K_{ML} along an average cycle on the attractor. The latter increase comes from a larger contribution from fine structures at frequencies exceeding f_c (within Regions 2 and 3). Fig. 21 gives that in the time series characterized by $D_{ML} > 5.5$, 20% or more of the energy of the signal appears as frequencies from Regions 2 and 3 of power spectra ($f_c > 2$ Hz). In the cases without a clear peak in the power spectrum, when no bottom bed exists, E_{WB} was calculated with $\Delta f < f < 0.5$ Hz, 2 Hz $< f < f_N$ and with 2 Hz $< f < f_N$, and no principal difference was obtained (except the shift in E_{WB} to lower energies for the latter case) as seen from Fig. 20. E_{WB} according to Eq. (23) was, therefore, used in all cases.

Figs. 20 and 21 indicate that the average cycle frequency cannot be used as a division between macro and finer structures of the time series in the frequency domain. On the one hand, this could be expected, since there is no theoretical relation between the analyses in frequency domain (E_{WB}) and in state-space (K_{ML}), and the results from these methods have to be interpreted independently of each other. On the other hand, the strong correlation between K_{ML} and E_{WB} (Figs. 18 and 20) indicates a correct interpretation of the outcomes of the two methods in terms of the relation between macro and finer structures. Fig. 22 confirms that the use of f_c as demarcation between Regions 1 and 2 in the power spectrum yields no correlation between K_{ML} and E_{WB} (cf. Fig. 20).

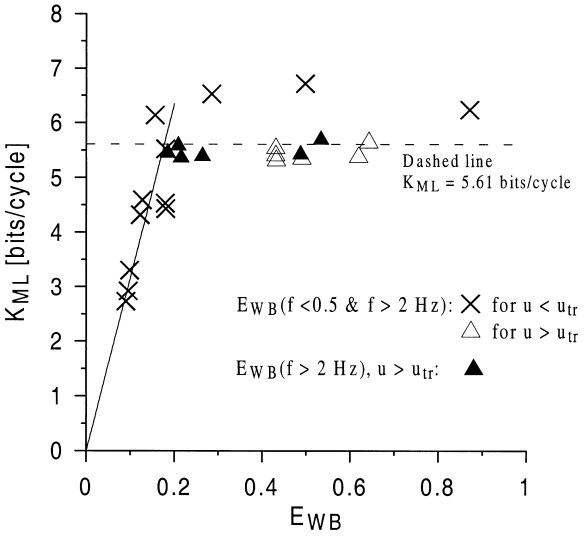

Fig. 20. Kolmogorov entropy (K_{ML}) in bits/cycle vs. the vide band energy (E_{WB}) for fluidized bed data.

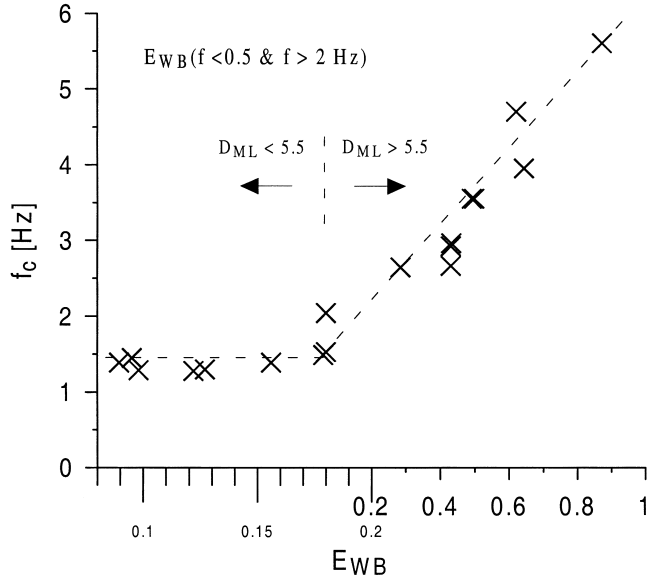

Fig. 21. Average cycle frequency (f_c) vs. wide band energy (E_{WB}) for the fluidized bed data.

The strong correlation between the wide band energy, E_{WB}, and the Kolmogorov entropy, K_{ML}, which occurs at D_{ML} lower than 5.5, illustrates that a change in width of the power spectrum can be directly linked to a change in predictability of the signal on time scales which are shorter than the average cycle time ($1/f_c$). For D_{ML} greater than 5.5, the state-space analysis treats fluctuations on time scales shorter than the average cycle time as noise, i.e., K_{ML} in bits/cycle does not respond to changes in amount of energy at frequencies outside Region 1.

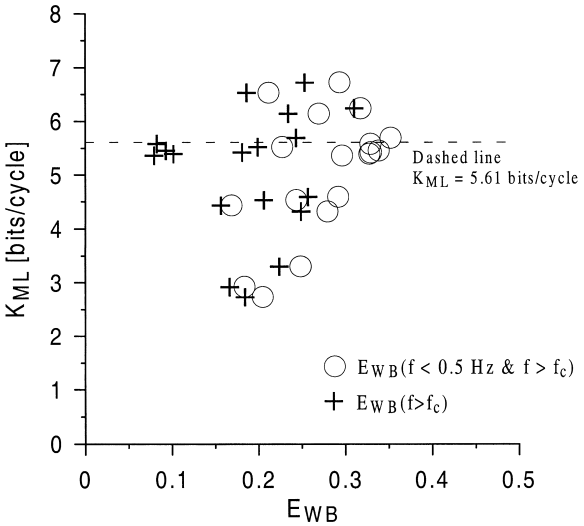

Fig. 22. Kolmogorov entropy (K_{ML}) in bits/cycle vs. the wide band energy (E_{WB}) with f_c as demarcation between Regions 1 and 2 in power spectra of the fluidized bed data.

In the latter case ($Z_{avg} > -3$, $D_{ML} > 5.5$), f_c corresponds to frequencies within Region 2, and there is a linear correlation between f_c and E_{WB} as shown in Fig. 21. When non-linearity can be proven, i.e., $Z_{avg} < -3$ and $D_{ML} < 5.5$, the average cycle frequency is within Region 1 in the spectrum ($f_c < 2$ Hz), Fig. 21.

The dimension of an attractor is not expected to be a direct function of the time scale of the system, and this is confirmed by Fig. 23 for $Z_{avg} \leftarrow -3$ (D_{ML} vs. E_{WB} yield a similar plot due to the relation between f_c and E_{WB} given in Fig. 21). As shown in Figs. 18, 20–22, the cases for which $D_{ML} > 5.5$ and $Z_{avg} > -3$ (Fig. 17), span over a wide range of total amount of energy in Regions 2 and 3 in the power spectrum. Within this span there are rather small variations in D_{ML} which, as in the case of the K_{ML} values, indicates that the state-space analysis does not respond to changes in amount of energy at frequencies outside Region 1 when $E_{WB} > 20\%$. Instead, the energy in these two regions is seen as noise.

Although there is a certain resemblance between the fall-off of the power spectrum (Fig. 15c) and the correlation dimension, D_{ML}, (Fig. 15d), the fall-off cannot be used to distinguish between non-linear time series ($Z_{avg} < -3$) and those which could not be distinguished from a linear (stochastic) time series ($Z_{avg} > -3$), Fig. 17. Thus, the method of using the fall-off in power spectrum to distinguish between low-dimensional (chaotic) and high-dimensional stochastic systems cannot be applied on the present fluidized bed data as was done on experimental time series from other types of systems (Brandstater and Swinney, 1987; Babloyantz and Destexhe, 1988; Philippou et al., 1991; el-Hamdi et al., 1993). As mentioned in Section 1.1, the method was also used on fluidized bed data (Nowak et al., 1993; Ding and Tam, 1994; Ding, 1997) with, according to our interpretation, results similar to those of the present study, i.e., the results are less clear-cut than from the other systems. Also, the method (cf. Section 1.1) of relating the exponential decay constant, μ, in a power spectrum to the sum of the positive Lyapunov exponents (i.e., to the Kolmogorov entropy), suggested and shown to

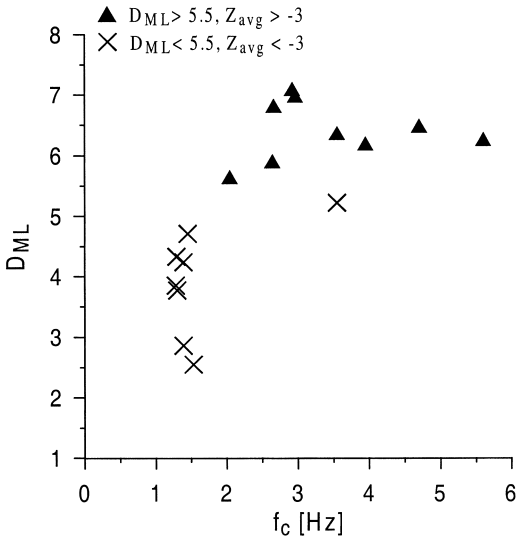

Fig. 23. Correlation dimension (D_{ML}) vs. average cycle frequency (f_c) for the fluidized bed data.

Table 3
Summary of the time-series analysis with respect to application and requirements for the study of fluidized bed hydrodynamics. The requirements may vary from case to case, and the figures given are applicable to the cases of the present work

Method	Criterion for regime identification	Data requirements number of samples, sampling frequency	Information which should be provided with the results[a]	Drawback(s)
Time domain (amplitude)	Identification of transition velocities (u_c and u_k) based on change in amplitude	1200, 20 Hz	Vertical pressure-drop profile	Indirect measure of dynamics
Frequency domain	Change in frequency distribution	$> 16 \times 1024$, 20 Hz (for dominant range of frequencies)	Number of spectra averaged, vertical pressure-drop profile	Interpretation of power spectra somewhat subjective
State-space	Change in K_{ML} and/or D_{ML}	$65{,}536 \approx 100$ times f_c, typically 100–600 Hz[b]	Vertical pressure-drop profile	Still under development, no standard software packages available

[a] It is assumed that number of samples and sample frequency is given.
[b] See Vander Stappen (1996) for details.

be approximately valid for modeled time series by Sigeti (1995b), was not applicable to the measured data of this work.

4.5. User guideline

The complex nature of the two-phase flow in fluidized beds with different regimes and applications makes it difficult to establish a standard way for employing the analysis methods discussed in this work. Table 3 gives a rough grading of the methods with respect to regime identification, amount of data needed for the analysis, what should be given in connection to the results and possible drawbacks of the methods. Especially in industrial applications, it is important to use as simple a method of analysis as possible.

Provided the amplitude (standard deviation) is used *together* with the pressure drop distribution (to identify change in the vertical extension of the dense bottom zone), it constitutes a simple method (cf. data requirements, Table 3) for a qualitative interpretation of changes in the flow regime. Important is to have a dense enough spacing of the pressure taps in order to identify change in the vertical extension of the dense bottom zone.

For the frequency domain analysis it is essential to average a sufficient number of spectra to ensure a high statistical significance. The results should always be accompanied with information on number of spectra averaged, sample frequency and length (number of samples) of each spectra. The sample frequency (and total number of samples) should be adjusted to the range of frequencies of interest. Thus, if only the major (bubble) frequencies are of interest (Region 1 of spectrum) a sampling frequency of 20 Hz would be sufficient in most cases. From previous experience, and also applicable for the data given in this work, is found that averaging at least 16 sub-spectra, each based on 1024 samples from 20 Hz sampling is sufficient. If, on the other hand, finer structures are of interest (Regions 2 and 3), obviously a higher sampling frequency has to be employed, but the total sampling time can be lowered. For interpretation of finer structures of the dynamics, the response time of the measurement system (pressure transducer and pressure tap) becomes of importance.

A possible advantage of the state-space analysis is that it may provide quantitative numbers for a description of the dynamics. The analysis is still under development, however, and commercially wide-spread software (for general purpose) lacks. A recent development (and necessary component in the analysis) is the non-linearity test described in Section 3.3. Vander Stappen (1996) recommends at least 65,536 samples to be taken at 100 points per cycle ($100 \times f_c$), typically yielding 150–600 Hz sampling frequency for the conditions of the present work. Vander Stappen gives a more detailed investigation on the accuracy of the state-space analysis with respect to number of samples and sample frequency.

5. Conclusions

Fluidization regimes are characterized by the major fluctuations of the flow, the macro-flow, which are linked to the visual appearance of the flow. There is a growing interest to analyze

the finer structures of the gas and solids flow. This calls for a description of the flow, which includes frequencies above those which are normally used for the definition of the fluidization regime. The present analysis, employing linear (time and frequency domain) and non-linear (state-space) time-series analysis of pressure fluctuations, emphasizes that the finer structures of the flow are important for a deeper understanding of two-phase flow dynamics.

5.1. Characterization of the flow regimes

For a description of the dynamics of the flow based on experiments, time-series analysis has to be used together with time-averaged values of the vertical distribution of solids. In the case of a dense bottom bed (under non-circulating as well as circulating conditions), the average voidage and height of the bottom bed strongly influence the amplitude of the fluctuations, but not necessarily the dynamics (time scale) of the fluctuations (Fig. 15). On the other hand, there are cases with pronounced differences in dynamics, which are not seen in the time-averaged quantities (Fig. 6 and Table 1).

The amplitude of pressure fluctuations (Table 1 and Fig. 15a), which is commonly used in regime studies, gives no direct information on the dynamics of the flow. A change in amplitude can be caused by a redistribution of solids in the fluidization system without any significant change in the dynamics of the flow. However, used together with the time-averaged vertical distribution of solids, the amplitude may still constitute a simple tool for regime characterization.

From the frequency domain analysis three characteristic regions were identified in the power spectrum of the measured in-bed pressure signals (Fig. 11Fig. 12):

Region 1. A region corresponding to the macro-structure of the flow in which the dominant frequencies are present. The distribution and amount of energy in this region differ significantly between the fluidization regimes studied. The region ranges typically up to about 4 Hz and is best presented on a linear scale as in Fig. 10.

Region 2. A region from about 4 to 10 Hz with a fall-off in frequency, which can be fitted either as a power-law or as an exponential fall-off. The fall-off is approximately in the same range ($\alpha = 1.9$–2.9) for the four regimes (Table 2) and is governed by finer structures of the flow.

Region 3. A region from about 20 to 200 Hz (the Nyquist frequency) with a power-law fall-off of $\alpha = 4.0$–5.4. This is a region with no clear dependence on the fluidization regime.

High-pass filtering revealed a pronounced intermittency in all cases studied, especially at high frequencies corresponding to Region 3 with $\alpha > 3$ (cf. Davis et al., 1994). The fluidized bed time series, which were proven non-linear with the highest statistical significance (single bubble regime), had the strongest intermittency (Figs. 13 and 14). With an increase in velocity within one regime, the dominant frequency (Fig. 15b), but also the distribution of energy in Region 1 of the power spectrum (Fig. 10), may appear to be independent of velocity in spite of a significant shift of energy up into the intermittent Regions 2 and 3 (Fig. 15e).

The presence of intermittency and the shape of the power spectra in Regions 2 and 3, together with the high Reynolds numbers obtained for the gas-phase flow (based on the bubble diameter, Table 1), makes the measured dynamics resemble that of gas-phase turbulence. Since

pressure was measured, the gas and solids phases cannot be separated and further studies are needed in order to investigate the origin and nature of the fluctuations in both phases.

5.2. Comparison of analysis in frequency domain and in state-space

Interpretation of the results in frequency domain and in state-space can be used complementary to each other. A key in the comparison is the non-linearity test which, for the system studied, shows that non-linearity cannot be proven when the correlation dimension, D_{ML}, exceeds 5.5 (Fig. 17). When $D_{ML} < 5.5$, non-linearity was proven, and there is a proportionality between the information loss in state-space, K_{ML}, and the amount of energy, E_{WB}, in Regions 2 and 3. Higher the E_{WB} higher the K_{ML}, and the lower is the predictability (Figs. 18 and 20). When $D_{ML} > 5.5$, K_{ML} is about 5.6 bits/cycle and is independent of cycle frequency and of E_{WB} (Figs. 19 and 20). The latter occurred for $E_{WB} > 20\%$ of the total amount of energy. In these cases, there are also only small changes in D_{ML} (Figs. 21 and 23) and the cycle frequencies, f_c, are outside of Region 1 of the power spectrum, $f_c > 2$ Hz. When an increase in complexity of the time series occurs at frequencies which are within Regions 2 and 3, the increase is not reflected in the state- space analysis, since $D_{ML} > 5.5$. In these cases ($f_c > 2$ Hz), f_c is proportional to E_{WB} (Fig. 21).

As a consequence, the state-space analysis is most appropriate in low-dimensional cases, when $D_{ML} < 5.5$. Otherwise, when $D_{ML} > 5.5$, the state-space analysis interprets the time series as if they were reconstructed from a system of many modes, and substantial changes in the energy distribution with respect to time-scale are not reflected in the analysis. However, K_{ML} expressed in bits/s will still give a qualitative response to changes in the time scale distribution (Fig. 18). It is not known if the major contribution to the lack of sensitivity in the state-space analysis, for $D_{ML} > 5.5$, is due to a high noise level ($E_{WB} > 20\%$) or to the fact that the actual number of modes is large.

The relation between the intermittency and the outcome of the non-linearity test should be further investigated. Of special interest is to include other simulated deterministic time series, such as the Lorenz-4D system. Filtering of the time series prior to the state-space analysis may also yield information on the influence of the noise (E_{WB}) on the outcome of the analysis.

The fluidized bed time series treated in this work (the four cases of Table 1) are available from http://www.entek.chalmers.se/ ~ fijo and results from analysis of them may be published, provided the source is given.

Acknowledgements

This work was financed by the Netherlands Organization for Scientific Research (NWO) and the Swedish National Energy Administration.

References

Abarbanel, H.D.I., 1996. Analysis of Observed Chaotic Data. Springer-Verlag, New York.

Abarbanel, H.D.I., Brown, R., Kadtke, J.B., 1990. Prediction in chaotic nonlinear systems: methods for time series with broadband Fourier spectra. Physical Review A 41, 1742–1807.

Abarbanel, H.D.I., Brown, R., Sidorowich, J.J., Tsimring, L.S., 1993. The analysis of observed chaotic data in physical systems. Rev. Modern Physics 65, 1331–1392.

Ahlers, G., Behringer, R.P., 1978. The Rayleigh–Bénard instability and the evolution of turbulence. Suppl. Progress of Theoretical Physics 64, 186–201.

Argyris, J., Faust, G., Haase, M., 1994. An Exploration of Chaos, Volume VII of Texts on Computational Mechanics. Elsevier, Amsterdam.

Avidan, A.A., Yerushalmi, J., 1982. Bed expansion in high velocity fluidized beds. Powder Technol. 32, 223–232.

Babloyantz, A., Destexhe, A., 1988. Is the normal hart a periodic oscillator? Biol. Cybernetics 58, 203–211.

Baker, G.L., Gollub, J.P., 1996. Chaotic Dynamics — An Introduction, 2nd ed. Cambridge University Press, New York.

Batchelor, G.K., 1959. The Theory of Homogeneous Turbulence. Cambridge University Press, Cambridge.

Bendat, J.S., Piersol, A.G., 1971. Random Data-Analysis and Measurement Procedures. Wiley/ Interscience, New York.

Bergh, H., Tijdeman, H., 1965. Theoretical and experimental results for the dynamic response of pressure measuring systems. Report NLR-TR F. 238, National Aeronautical and Astronautical Research Institute, Amsterdam.

Bi, H., Fan, L.-S., 1992. Existence of turbulent regime in gas–solid fluidization. AIChE J. 38, 297–301.

Bi, H.T., Grace, J.R., 1995. Effect of measurement method on the velocities used to demarcate the onset of turbulent fluidizaion. Chem. Eng. J. 57, 261–271.

van den Bleek, C.M., Schouten, J.C., 1993. Deterministic chaos: a new tool in fluidized bed design and operation. Chem. Eng. J. 53, 75–87.

Brandstater, A., Swinney, H.L., 1987. Strange attractors in weakly turbulent Couette–Taylor flow. Physical Review A 35, 2207–2220.

Broadhurst, T.E., Becker, H.A., 1976. Measurement and spectral analysis of pressure fluctuations in slugging beds. In: Keairns, D.L. (Ed.), Fluidization Technology, vol. 1. Engineering Foundation, New York, pp. 63–85.

Canada, G.S., McLaughlin, M., Staub, F.W., 1978. Flow regimes and void fraction distribution in gas fluidization of large particles in beds without tube banks. AIChE Symp. Series 74 (176), 14–26.

Casdagli, M., des Jardins, D., Eubank, S., Farmer, J.D., Gibson, J., Theiler, J., Hunter, N., 1992. In: Kim, J.H., Stringer, J. (Eds.), Applied Chaos. Wiley, New York, pp. 335–380.

Daw, C.S., Halow, J.S., 1991. Characterization of voidage and pressure signals from fluidized beds using deterministic chaos theory. In: Anthony, E.J. (Ed.), Proc. Eleventh Int. Conf. Fluidized Bed Combustion. American Society of Mechanical Engineers, New York, pp. 777–786.

Davis, A., Marshak, A., Wiscombe, W., Cahalan, R., 1994. Multifractal characterizations of nonstationarity and intermittency in geophysical fields: observed, retrieved or simulated. J. Geophysical Research 99, 8055–8072.

Ding, J., 1997. Analysis of hydrodynamic and chemical reactons in circulating fluidized beds. In: Kwauk, M., Li, J. (Eds.), Circulating Fluidized Bed Technology V. Science Press, Beijing, pp. 446–451.

Ding, J., Tam, S.-W., 1994. Asymptotic power spectrum analysis of chaotic behavior in fluidized beds. Int. J. Bifurcation and Chaos 4, 327–341.

Eckmann, J.-P., Oliffson-Kamphorst, S., Ruelle, D., Ciliberto, S., 1986. Liapunov exponents from time series. Physical Review A 34, 4971–4979.

el-Hamdi, M., Gorman, M., Robbins, K.A., 1993. Deterministic chaos in laminar premixed flames: experimental classification of chaotic dynamics. Comb. Sci. Tech. 94, 87–101.

Fan, L.T., Ho, T.-C., Hiraoka, S., Walawender, W.P., 1981. Pressure fluctuations in a fluidized bed. AIChE J. 27, 388–396.

Farabee, T.M., Casarella, M.J., 1991. Spectral features of wall pressure fluctuations beneath turbulent boundary layers. Phys. Fluids A 3, 2410–2420.

Frisch, U., Morf, R., 1981. Intermittency in nonlinear dynamics and singularities at complex times. Physical Review A 23, 2673–2705.

George, W.K., Beuther, P.D., Arndt, R.E.A., 1984. Pressure spectra in turbulent free shear flows. J. Fluid Mech. 148, 155–191.

Glicksman, L.R., Hyre, M., Woloshun, K., 1993. Simplified scaling relationships for fluidized beds. Powder Technol. 77, 177–199.
Grassberger, P., Procaccia, I., 1984. Dimensions and entropies of strange attractors from a fluctuating dynamics approach. Physica 13D, 34–54.
Grassberger, P., Procaccia, I., 1983a. Estimation of the Kolmogorov entropy from a chaotic signal. Physical Review A 28, 2591–2593.
Grassberger, P., Procaccia, I., 1983b. Characterization of strange attractors. Phys. Rev. Lett. 50, 346–349.
Grassberger, P., 1986. Estimating the fractal dimensions and entropies of strange attractors. In: Holden, A.V. (Ed.), Chaos-Nonlinear Science: Theory and Applications. Manchester University Press, Manchester, pp. 291–311.
Greenside, H.S., 1997. Department of Computer Science and Department of Physics, Duke University, Durham, private communication.
Greenside, H.S., Ahlers, G., Hohenberg, R.C., Walden, R.W., 1982. A simple stochastic model for the onset of turbulence in Rayleigh–Bérnard convection. Physica 5D, 322–334.
Hay, J.M., Nelson, B.H., Briens, C.L., Bergougnou, M.A., 1995. The calculation of the characteristics of a chaotic attractor in a gas–solid fluidized bed. Chem. Eng. Sci. 50, 373–380.
Hilborn, R.C., 1994. Chaos and Nonlinear dynamics — An Introduction For Scientists and Engineers. Oxford University Press, New York.
Johansson, B., 1997. Department of Thermo and Fluid Dynamics. Chalmers University of Technology, Göteborg, private communication.
Johnsson, F., Andersson, S., Leckner, B., 1991. Expansion of a freely bubbling fluidized bed. Powder Technol. 68, 117–123.
Johnsson, F., Leckner, B., 1995. Vertical distribution of solids in a CFB-furnace. In: Heinschel, K.J. (Ed.), Proc. Thirteenth Int. Conf. Fluidized Bed Combustion. American Society of Mechanical Engineers, New York, pp. 671–679.
Johnsson, F., Svensson, A. Andersson, S., Leckner, B., 1995. Fluidization regimes in boilers, Fluidization VIII (preprints), Tours, 129-136.
Johnsson, F., Svensson, A., Leckner, B., 1992. Fluidization regimes in circulating fluidized bed boilers. In: Potter, O.E., Nicklin, D.J. (Eds.), Fluidization VII. Engineering Foundation, New York, pp. 471–478.
Kennel, M.B., Isabelle, S., 1992. Method to distinguish possible chaos from colored noise and to determine embedding parameters. Physical Review A 46, 3111–3118.
Kikuchi, R., Tsutsumi, A., Yoshida, K., 1997. Stochastic analysis of bubble and particle motions in a 2D three-phase reactor. J. Chem. Eng. Japan 30, 202–209.
Kuo, A.Y.-S., Corrsin, S., 1971. Experiments on internal intermittency and fine-structure distribution functions in fully turbulent fluid. J. Fluid. Mech. 50, 285–319.
Lee, G.S., Kim, S.D., 1988. Pressure fluctuations in turbulent fluidized beds. J. Chem. Eng. Japan 28, 515–521.
Letaief, N., Rozé, C., Gouesbet, G., 1995. Noise/chaos distinction applied to the study of a fluidized bed. J. Physique II France 5, 1883–1899.
Li, Y., Kwauk, M., 1980. The dynamics of fast fluidization. In: Grace, J.R., Matsen, J.M. (Eds.), Fluidization. Plenum Press, New York, pp. 537–544.
Lirag, R.C., Littman, H., 1971. Statistical study of the pressure fluctuations in a fluidized bed. Chem. Eng. Prog. Symp. Series 67, 11–22.
Livshits, Yu.E., Tamarin, A.I., 1980. Experimental investigation of fluctuations in the velocity of the solid phase in a fluidized bed. J. Eng. Phys. 39, 727–731.
Löfdahl, L., Kälvesten, E., Stemme, G., 1996. Small silicon pressure transducers for space–time correlation measurements in a flat plate boundary layer. J. Fluids Eng. 118, 457–463.
Lorenz, E.N., 1963. Deterministic nonperiodic flow. J. Atmos. Sci. 20, 130–141.
Lorenz, E.N., 1984. The local structure of a chaotic attractor in four dimensions. Physica 13D, 90–104.
Manneville, P., 1981. Statistical properties of chaotic solutions of a one-dimensional model for phase turbulence. Physics Letters 84A, 129–132.
Monin, A.S., Yaglom, A.M., 1975. Statistical Fluid Mechanics. MIT Press, New York.
Moon, F.C., 1992. Chaotic and Fractal Dynamics: An Introduction for Applied Scientists and Engineers. Wiley, New York.

Newby, R.A., Keairns, D.L., 1986. Test of the scaling relationships for fluid-bed dynamics. In: Ostergaard, K., Sorensen, A. (Eds.), Fluidization V. Engineering Foundation, New York, pp. 31–38.

Nicastro, M.T., Glicksman, L.R., 1984. Experimental verification of scaling relationships for fluidized bed. Chem. Eng. Sci. 39, 1381–1391.

Nowak, W., Matsuda, H., Win, K.K., 1993. Diagnosis of multi-solid fluidized beds by power spectrum analysis of pressure fluctuations. In: Avidan, A. (Ed.), Circulating Fluidized Bed Technology IV. Hidden Valley, Pennsylvania, pp. 131–136.

van Ommen, J.R., Schouten, J.C., Vander Stappen, M.L.M., van den Bleek, C.M., 1999. Response characteristics of probe-transducer systems for pressure measurements in gas–solid fluidized beds: how to prevent pitfalls in dynamic pressure measurements. Powder Technol., accepted for publication.

Pemberton, S.T., Davidson, J.F., 1984. Turbulence in the freeboard of a gas-fluidised bed — the significance of ghost bubbles. Chem. Eng. Sci. 39, 829–840.

Press, W.H., Teukolsky, S.A., Vetterling, W.T., Flannery, B.P., 1992. Numerical Recipes in C. Cambridge University Press, Cambridge.

Provenzale, A., Villone, B., Babiano, A., Vio, R., 1993. Intermittency, phase randomization and generalized fractal dimensions. Int. J. Bifurcation and Chaos 3, 729–736.

Provenzale, A., Vio, R., Cristiani, S., 1994. Luminosity variations of 3C 345: is there any evidence of low-dimensional chaos? Astrophysical J. 428, 591–598.

Qureshi, A.E., Creasy, D.E., 1979. Fluidised bed gas distributors. Powder Technol. 22, 113–119.

Peirano, E., Palchonok, G., Johnsson, F., Leckner, B., 1998. Estimates of turbulence mechanisms in circulating fluidized bed combustors. Powder Technology 96, 90–105.

Philippou, G., Schultz, F., Luss, D., 1991. Spatiotemporal temperature patterns on an electrically heated catalytic ribbon. J. Phys. Chem. 95, 3224–3229.

Proakis, J.G., Manolakis, D.G., 1989. Introduction to Digital Signal Processing. Macmillan, New York.

Rabiner, L.R., Gold, B., 1975. Theory and Application of Digital Signal Processing. Prentice-Hall, Englewood Cliffs.

Rhodes, M.J., Geldart, D., 1986. Transition to turbulence? In: Østergaard, K., Sorensen, A. (Eds.), Fluidization V. Engineering Foundation, New York, pp. 281–288.

Saddoughi, S.G., Veeravalli, S.V., 1994. Local isotropy in turbulent boundary layers at high Reynolds number. J. Fluid Mech. 268, 333–372.

Satija, S., Fan, L.-S., 1985. Characteristics of slugging regime and transition to turbulent regime for fluidized beds of large coarse particles. AIChE J. 31, 1554–1562.

Satija, S., Young, J.B., Fan, L.-S., 1985. Pressure fluctuations and choking criterion for vertical pneumatic conveying of fine particles. Powder Technol. 43, 257–271.

Schewe, G., 1983. On the structure and resolution of wall-pressure fluctuations associated with turbulent boundary-layer flow. J. Fluid Mech. 134, 311–328.

Schouten, J.C., 1997. Non-Linear Short-Term Predictability in Time Series Measured in Gas–Solid Fluidized Beds Operated from Minimum Fluidization up to Dilute Transport, internal report. Department of Chemical Process Technology, Faculty of Chemical Technology and Materials Science, Delft University of Technology, Delft.

Schouten, J.C., Takens, F., van den Bleek, C.M., 1994a. Estimation of the dimension of a noisy attractor. Physical Review E 50, 3–13.

Schouten, J.C., Takens, F., van den Bleek, C.M., 1994b. Maximum likelihood estimation of the entropy of an attractor. Physical Review E 49, 126–129.

Schouten, J.C., Vander Stappen, M.L.M., van den Bleek, C.M., Daw, C.S., Lawkins, W.F., 1994, Comparison of DUT and ORNL nonlinear data analysis methods. EPRI Report CF 8006-092-17816, USA.

Schouten, J.C., Vander Stappen, M.L.M., van den Bleek, C.M., 1996. Scale-up of chaotic fluidized bed hydrodynamics. Chem. Eng. Sci. 51, 1991–2000.

Sigeti, D.E., 1996. Los Alamos National Laboratories, Los Alamos, private communication.

Sigeti, D.E., 1995a. Survival of deterministic dynamics in the presence of noise and the exponential decay of power spectra at high frequency. Physical Review E 52, 2443–2457.

Sigeti, D.E., 1995b. Exponential decay of power spectra at high frequency and positive Lyapunov exponents. Physica D 82, 136–153.

Sigeti, D.E., Horsthemke, W., 1987. High-frequency power spectra for systems subject to noise. Physical Review A 35, 2276–2282.

Skrzycke, D.P., Nguyen, K., Daw, C.S., 1993. Characterization of the fluidization behavior of different solid types based on chaotic time-series analysis of pressure signals. In: Rubow, L., Commonwealth, G. (Eds.), Proc. Twelfth Int. Conf. Fluidized Bed Combustion. American Society of Mechanical Engineers ASME Book No. I0344B, New York, pp. 155–166.

Stock, D.E., 1995. Particle dispersion in turbulent gas flows, In: Serizawa A., Fukano T., Bataille J. (Eds.), Proc. Second Int. Conf. Multiphase Flow, Kyoto, pp. PL2-1–PL2-13.

Svensson, A., Johnsson, F., Leckner, B., 1996a. Fluidization regimes in non-slugging fluidized beds: the influence of pressure drop across the air distributor. Powder Technol. 86, 299–312.

Svensson, A., Johnsson, F., Leckner, B., 1996b. Bottom bed regimes in a circulating fluidized bed boiler. Int. J. Multiphase Flow 22, 1187–1204.

Sun, J.G., Chen, M.M., Chao, B.T., 1994. Modeling of solids global fluctuations in bubbling fluidized beds by standing surface waves. Int. J. Multiphase Flow 20, 315–338.

Takens, F., 1993. Detecting nonlinearities in stationary time series. Int. J. Bifurcation and Chaos 3, 241–256.

Takens, F., 1985. On the numerical determination of the dimension of an attractor. In: Braaksma, B.L.J., Broer, H.W., Takens, F. (Eds.), Proc. Dynamical Systems and Bifurcations, Lecture Notes in Mathematics 1125. Springer Verlag, Berlin, pp. 99–106.

Takens, F., 1981. Detecting strange attractors in turbulence. In: Rand, D.A., Yong, L.S. (Eds.), Proc. Dynamical Systems and Turbulence, in Lecture Notes in Mathematics 898. Springer Verlag, Berlin, pp. 366–381.

Tam, S.W., Devine, M.K., 1989. Is there a strange attractor in a fluidized bed? In: N.B. Abraham, A.M. Albano, A. Passamante, P.E. Rapp (Eds.), Measures of Complexity and Chaos. Plenum, New York, pp. 193–197.

Tamarin, A.I., Livshits, Yu.E., 1977. A Study of Local Characteristics of Gas motion in a Fluidized Bed of Large Particles. Izvestiya Academii Nauk B.S.S.R., Ser. Fiz.-Energ. Nauk 3, 129–130.

Tennekes, H., Lumley, J.L., 1972. A First Course in Turbulence. MIT Press, Cambridge, MA.

Tessier, Y., Lovejoy, S., Schertzer, D., 1993. Universal multifractals: theory and observations for rain and clouds. J. Applied Meteorology 32, 223–250.

Vander Stappen, M.L.M., 1996. Chaotic hydrodynamics of fluidized beds. Thesis, Delft University Press, Delft.

Vander Stappen, M.L.M., Schouten, J.C., van den Bleek, C.M., 1993. Application of deterministic chaos theory in understanding the fluid dynamic behavior of gas–solids fluidization. AIChE Symp. Series 89 (296), 91–102.

Verloop, J., Heertjes, P.M., 1974. Periodic pressure fluctuations in fluidized beds. Chem. Eng. Sci 29, 1035–1042.

Welch, P.D., 1967. The use of a fast Fourier transform for the estimation of power spectra. IEEE Trans. Audio and Electroacoustics AU-15, 70–73.

Yang, W.C., Ettehadieh, B., Anestis, T.C., Gizzie, R.E., Haldipur, G.B., 1986. Fluidization phenomena in a large jetting fluidized bed. In: Ostergaard, K., Sorensen, A. (Eds.), Fluidization V. Engineering Foundation, New York, pp. 95–102.

Yerushami, J, Avidan, A.A., 1985. High velocity fluidization. In: Davidson, J.F., Clift, R., Harrison, D. (Eds.), Fluidization. Academic Press, New York, pp. 225–291.

Zijerveld, R.C., Johnsson, F., Marzocchella, A., Schouten, J.C., van den Bleek, C.M., 1998. Fluidization regimes and transitions from fixed bed to dilute transport flow. Powder Tech. 95, 185–204.

Zijerveld, R.C., Johnsson, F., Marzocchella, A., Schouten, J.C., van den Bleek, C.M., 1997a. Chaotic hydrodynamics in the riser bottom zone of circulating fluidized beds of different size. In: Kwauk, M., Li, J. (Eds.), Circulating Fluidized Bed Technology. Science Press, Beijing, pp. 242–247.

Zijerveld, R.C., Koniuta, A., Johnsson, F., Marzocchella, A., Schouten, J.C., van den Bleek, C.M., 1997b. Axial solids distribution and bottom bed dynamics for circulating fluidized bed combustor application. AIChE Symp. Series 93 (317), 97–102.

Zuiderweg, F.J., 1967. Report. In: Drinkenburg A.A.H. (Ed.), Proc. of the Symposium on Fluidization. pp. 739–750.